2009

Development of extrusion on demand for ceramic freeze-form extrusion fabrication processes

Parimal Sanjay Kulkarni

Department:

DEVELOPMENT OF EXTRUSION ON DEMAND FOR CERAMIC FREEZE-FORM EXTRUSION FABRICATION PROCESSES

by

PARIMAL S. KULKARNI

A THESIS

Presented to the Faculty of the Graduate School of the

MISSOURI UNIVERSITY OF SCIENCE AND TECHNOLOGY

In Partial Fulfillment of the Requirements for the Degree

MASTER OF SCIENCE IN MANUFACTURING ENGINEERING

2009

Approved by

Ming C. Leu, Advisor
Robert G. Landers, Co-Advisor
Gregory E. Hilmas

PUBLICATION THESIS OPTION

This thesis consists of the following article that will be submitted for publication as follows:

The manuscript titled “Development of Extrusion on Demand for Ceramic Freeze-form Extrusion Fabrication Processes” on pages 7-59 will be submitted to the Journal of Materials Processing Technology.

ABSTRACT

Freeze-form Extrusion Fabrication (FEF) is a Solid Freeform Fabrication method. It involves the deposition of a ceramic paste in a layer by layer manner to construct a three dimensional structure. The ceramic paste used in this process consists of a high solids loading of ceramic powder mixed with water and a nominal amount of an aqueous organic binder. These characteristics make the process environmentally friendly. Also the absence of dies or molds in the process makes it suitable for fabrication of materials like ceramics. In the past, parts have been fabricated with continuous extrusion of a ceramic paste. In FEF, Extrusion on Demand (EOD) refers to the ability to control the start and stop paste extrusion on command. Extrusion on Demand makes possible the fabrication of parts with complex geometries and internal features. The extrusion force is an important aspect to be controlled for the successful implementation of EOD in FEF. A general tracking controller with integral action is implemented to allow precise tracking of the reference force. Two possible methods of achieving EOD by controlling extrusion force and fine tuning process parameters have been discussed. Experiments are conducted to tune the controller and process parameters. Working ranges for all process parameters have been established. Three dimensional ceramic structures have been fabricated by using the parameter values obtained from the experiments.

.

ACKNOWLEDGMENTS

I take this opportunity to thank my advisor Dr. Ming Leu for his guidance. I would like to thank my co-advisor Dr. Robert Landers for his advice, patience and thorough guidance throughout the course of his project. I would also like to thank my committee member, Dr. Gregory Hilmas for his suggestions.

My sincerest appreciation is extended to my colleague Thomas Oakes for his help in the completion of this research project. I also thank all my friends Joseph Ishaku, Mike Fleming and Lie Tang for their enthusiastic support.

I would like to express my gratitude to my parents whose love, encouragement and patience has been invaluable to me always and to my fiancé for his care, love and support in all of my endeavors.

TABLE OF CONTENTS

LIST OF ILLUSTRATIONS

LIST OF TABLES

Page

NOMENCLATURE

Symbol	Description
U	Command Voltage to Motor Amp (mV)
g_0, g_1	Controller Gains
D_{ext}	Extrudate Diameter (m)
τ_1, τ_2	Desired Extrusion Force Time Constants (s)
F	Extrusion Force (N)
a_0,b_0	Extrusion force model parameters
G	Extrusion Force Model Transfer Function
K	Extrusion Force Model Gain (N/mV)
τ	Extrusion Force Model Time Constant (s)
V_{ext}	Extrudate Velocity (m/s)
z	Forward Shift Operator
d_{gap}	Gap between Deposited Lines (m)
R	Reference Extrusion Force (N)
T	Sample Period (s)
η	Vector of Model Parameter Estimates
φ	Vector of Regression Variables

1. INTRODUCTION

The need for customized fabrication processes offering cost and time efficiency have led to extensive research of rapid prototyping methods for various materials. Amongst these methods extrusion based rapid prototyping offers the flexibility to fabricate customized components created with materials like ceramics and composites and are of special interest as they eliminate the necessity of tools or dies. Since these methods eliminate the need of material removal for fabricating parts they can be referred to as additive manufacturing techniques. Variants of this method are processes like Fused Deposition Modeling (FDM), Low-Temperature Deposition Manufacturing (LDM), Rapid Freeze Prototyping (RFP), Robocasting, Layered Manufacturing (LM) and Fused Deposition of Ceramics (FDC) (Calvert et al. 1993; Danforth et al. 1996; Cesarno, 2004; Bellini, 2002). Most of these extrusion based Solid Freeform Fabrication (SFF) methods can be used to fabricate three dimensional (3D) parts from CAD files directly (Danforth et al. 1996). This increases the possibility of automating the process and effectively decreases the time, cost and human intervention involved in the rapid prototyping process. Solid Freeform Fabrication methods like Selective Laser Sintering (SLS) combine extrusion deposition of ceramics/metallic powders with use of laser power for densification (Wang et al. 2002). Fused Deposition of Ceramics at hot temperatures has been used to fabricate parts using a filament consisting of ceramics, polymers, elastomer and wax (Danforth et al. 1996). Low-Temperature Deposition Manufacturing has been used to construct composite scaffolds for tissue engineering applications by depositing composite slurry at low temperature (Cesarno, 2004). Freeze-form Extrusion Fabrication (FEF) is an additive manufacturing technique that consists of layer by layer deposition of

ceramic paste at a temperature below the paste freezing temperature to create 3D structures (Zhao et al. 2007). Freeze-form Extrusion Fabrication has been developed using the basic idea behind RFP (Zhao et al. 2008). The ceramic paste contains a high volume of ceramic powder, uniformly mixed with water and a nominal amount of a water soluble organic binder. Freeze-form Extrusion Fabrication is more environmentally friendly than methods like FDC as it does not generate any harmful wastes during post processes (Wang and Shaw, 2005). In FEF the ceramic paste is deposited in a layer by layer manner by a ram extruder system mounted on a 3D gantry. The 3D gantry allows deposition in the X-Y direction. The motion in the Z direction allows the nozzle to move up the required nozzle height. A green part fabricated using FEF is freeze dried to remove the water, the binder is burned out and the part is sintered to give it mechanical strength and stability. Freeze-form Extrusion Fabrication has been implemented previously to build successful parts with continuous extrusion. Development of FEF extrusion on demand allows fabrication of parts with complex geometries.

The ceramic paste used for fabricating successful parts is an important aspect of development of extrusion on demand in FEF. In the FEF process the paste needs to be pseudo plastic /shear thinning in nature. Pseudo plasticity is a property exhibited by some materials in which the viscosity of the material decreases with increase in the shear force. Pseudo plasticity is a basic requirement for obtaining extrudates with rectangular cross sections because the paste solidifies in place once the shear stress is removed as the paste exits the nozzle tip (Yang et al. 2006). In FEF the pseudo plasticity of the paste is regulated with the help of binder content or by adjusting the pH value of the paste.

Study of the process parameters related to extrusion fabrication is essential to successfully develop any deposition process which uses paste that is pseudo plastic in nature. Some of these process parameters are the standoff distance, table velocity and extrudate velocity (Cesarno et al. 2004). Wang and Shaw (2002) discussed the effect of the nozzle height on the cross sectional geometry of extrudates and developed an equation relating standoff distance to extrudate velocity, table velocity and nozzle diameter for paste deposition processes. For multi-layered single walled parts Wang and Shaw (2002) used a nozzle height less than the standoff distance to obtain the required extrudate cross sectional geometry. In FEF various standoff distances are experimented with, till an appropriate working range has been established. Yang et al. (2008) developed a formula for establishing the table velocity as a function of ram diameter, nozzle diameter and extrudate velocity. It was established that extrudate velocities less than the table velocity leads to stretching of the deposited extrudate and extrudate velocity greater than the table velocity leads to non-uniform deposition of the extrudate. Benbow and Bridgewater (1992) developed an equation relating the average extrusion pressure to the paste velocity during steady-state extrusion. From various studies it can be concluded that the process parameters need to be optimized for creating dense parts such that the deposited extrudate is flattened into rectangular cross sections.

Freeze-form Extrusion Fabrication relies on modeling and control of the ram extrusion process to obtain the desired extrusion quality and part fabrication. Amarasinghe and Wilson (1998) stated that ceramics based pastes are generally more difficult to extrude as compared to polymers due to inconsistencies in the paste properties in both the paste creation and extrusion processes. In FEF feedback control has been

implemented to account for these inconsistencies (Zhao et al. 2008). Most studies related to extrusion based rapid prototyping discuss continuous extrusion. Most processes, except Robocasting, use a polymer-ceramic mix for better extrusion control and quality. A study conducted by Mason et al. (2007) investigated the feasibility of a start-stop controller with force control. More research is required in this area to fine tune the extrusion process to fabricate parts with complex geometries and internal features.

The focus of this research is the development of extrusion on demand in FEF. In the past, parts have been fabricated using continuous extrusion. Complex geometries can be fabricated using various methods like building parts with overhangs by controlling the pH and elasticity of paste as demonstrated by Wang and Shaw (2006). Wu et. al (2001) demonstrated the fabrication of complex parts using metal powders and binders with continuous flow of material. With the development of extrusion on demand in FEF, ceramic pastes with low binder concentrations can now be used to fabricate parts with internal holes, complex geometries. The need for adding polymers or controlling paste properties to modify the behavior of ceramic pastes to achieve satisfactory start and stop has been eliminated. The use of aqueous pastes and a low concentration of organic binder make the FEF process more environmentally friendly.

REFERENCES

1. Agarwala, M.K., Bandopadhyay, A., Weeren, R., Safari, A., Danforth, S.C., Langrana, N.A., Jamalabad, V., and Whalen P.J., 1996, FDC, Rapid Fabrication of Structural Components, The American Ceramic Society Bulletin, Vol. 65, pp. 60-65.

2. Amarasinghe, A.D.U.S. and Wilson, D.I., 1998, Interpretation of Paste Extrusion Data, Chemical Engineering Research and Design, Vol.76, No. (A1), pp. 3-8.

3. Bellini, A., 2002, Fused Deposition of Ceramics: A Comprehensive Experimental, Analytical and Computational Study of Material Behavior, Fabrication Process and Equipment Design, PhD. Dissertation, Drexel University, Department of Mechanical Engineering.

4. Benbow, J.J., and Bridgewater, J., 1992, Paste Flow and Extrusion, Clarendon Press, Oxford.

5. Calvert, P., Lombardi, J., Mulligan, A., and Stuffle, K., 1993, Solid Freebody Forming from Polymerizable Slurry, Proceedings of Solid Freeform Fabrication Symposium, Austin, Texas, pp. 60-63.

6. Cesarano, J., King, B., and Denham, H.B., 2004, Recent Developments in Robocasting of Ceramics and Multimaterial Deposition, Proceedings of Solid Freeform Fabrication Symposium, Austin, Texas, pp. 679-703.

7. Huang, T.S., Mason, M.S., Hilmas, G.E., and Leu, M.C., 2006, Freeze-form Extrusion Fabrication of Ceramics, Virtual and Physical Prototyping, Vol. 1 (2), pp. 93-100.

8. Mason, M.S., Huang, T., Leu, M.C., Landers, R.G., and Hilmas, G.E., 2007, Aqueous–Based Extrusion Fabrication of Ceramics on Demand, Solid Freeform Fabrication Symposium Proceedings, Austin, Texas, pp. 124-134.

9. Wang, J. and Shaw, L., 2005, Rheological and Extrusion Behavior of Dental Porcelain Slurries for Rapid Prototyping Applications, Materials Science and Engineering A, Vol. 397, No.1-2, pp. 314-321.

10. Wu, G., Langrana, N.A., Sadanji, R., Danforth, S., 2001, Solid freeform fabrication of metal components using fused deposition of metals, Materials & Design, Vol. 23, No.1, pp. 97-105.

11. Xiong, Z., Yan, Y., Wang, S., Zhang, R., and Zhang, C., 2002, Fabrication of Porous Scaffolds for Bone Tissue Engineering via Low Temperature Deposition, Scripta Materialia, Vol. 46, No. 11, pp. 771-776.

12. Yang, S., Yang, H., and Evans J.R.G., 2006, Direct Extrusion FreeForming of Ceramic Pastes, Solid Freeform Fabrication Symposium Proceedings, Austin, Texas, pp. 304-315.

13. Yang, S., Yang, H., Evans, J.R.G., Chi, X., Thompson, I., Cook, R.J., and Robinson, P., 2008, Rapid Prototyping of Ceramic Lattices for Hard Tissue Scaffolds, Materials and Design, Vol. 29, pp. 1802-1809.

14. Zhao, X., Landers, R.G., and Leu, M.C., 2008, Adaptive Control of Freeze–form Extrusion Fabrication Processes, ASME Dynamic Systems and Controls Conference, Ann Arbor, Michigan.

15. Zhao, X., Mason, M.S., Huang, T.S., Leu, M.C., Landers, R.G., Hilmas, G.E., Easley, S.J. and Hayes, M.W., 2007, Experimental Investigation of Effect of Environment Temperature on Free-form Extrusion Fabrication, Solid Freeform Fabrication Symposium Proceedings, Austin, Texas, pp. 135-146.

PAPER

I. Development of Extrusion on Demand for Ceramic Freeze-form Extrusion Fabrication Process

Parimal Kulkarni, Thomas Oakes, Ming C. Leu, Robert G. Landers

Missouri University of Science and Technology

Department of Mechanical and Aerospace Engineering

400 West 13th Street, Rolla, Missouri 65409-0050

{pskf44;tmo6w3;landersr;mleu}@mst.edu

Abstract

In the Freeze-form Extrusion Fabrication (FEF) process, Extrusion-on-Demand (EOD) refers to the ability to control the start and stop of paste extrusion, which is vital to the fabrication of parts with complex geometries. Control of the extrusion force can be used in FEF to regulate the flow of extruded material and achieve EOD. This paper discusses two approaches of developing EOD through modeling and control of the extrusion force and selection of appropriate process parameters. A general tracking controller with integral action is used to allow precise tracking of a variety of reference forces, while accounting for the inherent variability in the paste properties. Experiments are conducted to tune the controller and process parameters. The results of the experiments are used to establish working ranges of the process parameters, and these values are used to fabricate various cross sections and complex parts. Post processes are conducted on the fabricated green parts. The fabricated structures establish that EOD has been successfully developed.

Keywords

Ceramics, Extrusion on Demand, Alumina, Zirconium Diboride, Rapid Prototyping

1. Introduction

Solid Freeform Fabrication (SFF), also referred to as Additive Manufacturing, is a process used to fabricate three dimensional (3D) parts without the use of molds or dies. Freeze-form Extrusion Fabrication (FEF) is one such SFF process which involves the extrusion of ceramic based pastes with high solids loading in a layer-by-layer manner for part fabrication. The green part obtained after fabrication is vacuum freeze-dried, the binder is removed through burnout, and high temperature pressure-less sintering is conducted to obtain the final part. This manufacturing method is inexpensive and efficient as compared to other ceramic fabrication methods for low quantity production or fabrication of parts with complex geometries because the FEF process is tool-less and does not require mold preparation. Low binder concentration in the aqueous based paste makes FEF an environmentally friendly manufacturing process. The process also conserves material as compared to conventional processes that rely on material removal methods.

Alumina (Al_2O_3, a higher temperature ceramic) or zirconium diboride (ZrB_2, an ultra high temperature ceramic) paste is utilized in the experiments conducted in this paper. The paste is a combination of mainly ceramic powder and water, with small amounts of binder, dispersant and lubricant. The ceramic solids loading are up to 50 vol. % of the paste volume. Water is the main liquid medium and the organic binder content is only approximately 2-4 vol. %.

A ram extruder mechanism is used extrude the ceramic paste in a layer-by-layer manner. The extruder is mounted on a 3D gantry system. Motions in the X-Y directions are used to fabricate each layer, and the extruder moves up a distance equal to one layer thickness after depositing each layer until fabrication is complete. The experimental setup is shown in Figure 1.

A detailed study and analysis of process parameters is essential to successfully develop any paste deposition process. Cesarno et al. (2004) and Danforth et al. (1996) discussed part fabrication using Robocasting and Fused Deposition of Ceramics with continuous extrusion and listed some of the critical process parameters as standoff distance, table velocity and extrudate velocity. Wang et al. (2002) discussed the effect of the nozzle height (standoff distance) on the cross sectional geometry of extrudates and developed an equation relating standoff distance to extrudate velocity, table velocity and nozzle diameter for paste deposition processes. For multi-layered single walled parts Wang and Shaw (2005) used a nozzle height less than the standoff distance to obtain the required rectangular cross sectional geometry of the extrudate. In FEF various standoff distances are analyzed, till an appropriate working range has been established. Yang et al. (2006) developed a formula for establishing the table velocity as a function of ram diameter, nozzle diameter and extrudate velocity. It was established that extrudate velocities less than the table velocity leads to stretching of the deposited extrudate and extrudate velocities greater than the table velocity leads to non-uniform deposition of the extrudate. Benbow and Bridgewater (1992) developed an equation relating the average extrusion pressure to the paste velocity during steady-state extrusion. From various

studies it can be concluded that the process parameters need to be optimized for creating dense parts such that the deposited extrudate is flattened into rectangular cross sections.

Dynamic modeling and control of the paste flow rate are major obstacles in the FEF process. Amarasinghe and Wilson (1998) stated that ceramic pastes are generally more difficult to extrude as compared to polymers due to inconsistencies in the paste properties in both the paste creation and extrusion processes. Mason et al. (2007) conducted studies on the paste dynamics and showed that it can be modeled as a first order dynamic process with significant variations in the time constant and gain. Another study (Mason et al., 2006) investigated the use of a bang-bang control strategy with feedback control of the extrusion force. Drawbacks of this method include excessive use of trial and error and lack of a systematic approach. Zhao et al. (2008) successfully conducted continuous extrusion fabrication with an adaptive extrusion force controller in the creation of a variety of ogive cones. The resulting parts were limited to shapes that could be made with continuous, single-line extrusion due to the absence of an EOD controller. A combination of logic inputs allowed for acceptable EOD during continuous motion on a case-by-case basis (Mason et al. 2007).

The objective of this paper is to develop a systematic method for EOD in FEF. The rest of the paper is organized as follows. First, the FEF experimental setup is described. Next, a dynamic extrusion model is constructed and used to design a general tracking controller with integral action to account for paste variability. The EOD methods are described in detail. The major FEF process parameters are introduced and discussed in detail, followed by experimental determination of their respective acceptable ranges.

Finally, a variety of two-dimensional cross-sections and 3D parts are fabricated and the results are described.

2. Experimental setup

The experimental platform consists of three subsystems: a 3-D gantry motion system, ram-extrusion mechanism, and temperature control system. The FEF system is shown in Figure 1. It consists of three Velmax BiSlide orthogonal linear axes, each containing limit and homing switches that allow 250 mm of travel. The X-axis consists of two parallel slides that support the weight of the remaining axes and extruder system. The Y-axis is mounted to top of the two X-axis slides, while the Z-axis is mounted to the Y-axis and the extruder mechanism is mounted to the Z-axis. Each of the four slides is powered by Pacific Scientific PMA22B motors with resolvers for position feedback. Each slide has a position resolution of 2.54 μm. All four signals sent from the respective resolvers are converted by resolver-to-digital encoders and serve as inputs to a Delta-Tau Turbo Programmable Multi-Axis Controller (PMAC) PCI board for motion control. The PMAC control board is used for gantry position regulation.

The extruder setup schematic is shown in Figure 2. A Kollmorgen AKM23D DC motor with a 0.254 μm resolution resolver is used for driving the extruder ram. An Omega LC305-1KA load cell is mounted between the extruder and plunger to measure the extrusion force. The force signal is sent to a Delta-Tau ACC28 board where it is used for feedback control. The force has 2.2 N of resolution. The control signal is limited to ± 250 mV to prevent system damage. The axis command voltages are sent from 16 bit Digital to Analog Converters (DAC), each with a range of ±5V, to their respective

amplifiers. Control of the extruder ram is implemented through custom PLC programs in the PMAC control board.

The gantry and extrusion systems are housed inside a freezer with a condenser that maintains the environmental temperature at 0 °C. An Omega CN 132 temperature controller is used in conjunction with liquid nitrogen to control the environmental temperature between 0 and -30 °C. An Omega DP7002 temperature controller is used with heating tape and a custom sleeve assembly surrounding the material reservoir to maintain the paste reservoir temperature to prevent freezing prior to extrusion. The sleeve assembly is shown in Figure 3.

The setup is run through a virtual CNC program, NCX-1122, which accesses information in the PMAC language to allow use of G&M motion coding control. The extrusion force data is collected at a sampling frequency of 10 Hz for all experiments.

The paste is loaded into plastic syringes that use twist-on hypodermic needles. A stainless steel plunger is inserted into the syringe for connection to the ram drive. The plastic syringe is press-fit into a stainless steel sleeve, which attaches to the extruder assembly. This setup allows for quick and convenient reloading of both paste and nozzle, and prevents the plastic syringe from translating as the extruder ram advances and retracts. The stainless steel syringe provides a barrier between the heating coils and paste, providing uniform heat distribution.

3. Process Modeling

A series of tests are conducted by changing the command voltages and measuring the extrusion force to obtain a dynamic model for the FEF extrusion process as shown in Figures 4 (alumina paste) and 5 (zirconium diboride paste). The input is set to 250 mV

until the start of extrusion is visually confirmed. Once extruding, the system is subjected to a series of step changes in the command voltage, which is cycled seven times. A first order model for the extrusion force process is assumed (Zhao et al. 2008). The variable F is the extrusion force and U is the input voltage

$$G(z) = \frac{F(z)}{U(z)} = \frac{b(z)}{a(z)} = \frac{K(1-\exp(-T/\tau))}{z-\exp(-T/\tau)} = \frac{b_0}{z+a_0} \tag{1}$$

where b_0 and a_0 are model coefficients to be determined from experiments. Equation (1) is transformed into the following difference equation

$$F(i) = -a_0 F(i-1) + b_0 U(i-1) \tag{2}$$

The Recursive Least Squares (RLS) algorithm is implemented where the vector of regression variables is

$$\phi = \begin{bmatrix} -F(i-1) & U(i-1) \end{bmatrix}^T \tag{3}$$

and the vector of unknown variables is

$$\eta = \begin{bmatrix} a_0 & b_0 \end{bmatrix}^T \tag{4}$$

The model coefficients for alumina paste with viscosity $280 \cdot 10^5$ cP at a shear rate of 101.893 s^{-1} and shear exponent 0.131 are determined to be a_0 = -0.998 and $b_0 = 3.97 \cdot 10^{-2}$ The model coefficients for zirconium diboride paste with viscosity $240 \cdot 10^5$ cP at a shear rate 101.893 s^{-1} of with shear exponent 0.109 are determined to be a_0 = -0.9914 and b_0 = $6.3 \cdot 10^{-2}$. $K_a = 1.9 \cdot 10^{-2}$ kN/mV, $K_z = 3.16 \cdot 10^{-2}$ kN/mV are the extrusion force gains for alumina and zirconium diboride respectively, T = 0.1 s is the sample period, τ_a = 42.7 s, and τ_z = 11.57 s are the time constants. The model is simulated with the data collected from the experiment. The input profile and results for alumina and zirconium diboride are shown in Figures 4 and 5 respectively. The model in equation (1) yields a maximum

absolute error of 155 N and an average absolute error of 17 N for alumina and a maximum absolute error of 35 N and an average absolute error of 3 N for zirconium diboride. A second experiment is conducted for validation of the dynamic extrusion model. The input profile, response and model predictions are shown in Figures 6 and 7. The model in equation (1) yields a maximum absolute error of 163 N and an average absolute error of 23 N and a maximum absolute error of 253 N and an average absolute error of 6 N. These values indicate that the first order process approximation is acceptable and can be used for controller design.

4. Controller Design

In this section, a control algorithm is designed to allow for EOD of the FEF process by developing a controller to extrude the paste consistently, as well as coordinate the start and stop of extrusion with the gantry motion.

A system block diagram of a general tracking controller is shown in Figure 8. A general tracking controller is designed to reject constant disturbances and regulate the extrusion force in real time with desired error dynamics. The extrusion force error dynamics are given by

$$\left[v(z)a(z)-g(z)\right]E(z)=0 \tag{5}$$

where $v(z)$ is the disturbance generating polynomial and is

$$v(z)=z-1 \tag{6}$$

and $E(z)$ is the extrusion force error and is

$$E(z)=R(z)-F(z) \tag{7}$$

where $R(z)$ is the reference extrusion force. The polynomial $a(z)$ is the denominator of the open-loop transfer function given in equation (5), and $g(z)$ is a first-order polynomial

$$g(z) = g_1 z + g_0 \tag{8}$$

where g_1 and g_0 are determined by the desired closed-loop error dynamics. Equation (5) can be rewritten as

$$\left[z^2 + (a - 1 - g_1)z + (-a - g_0)\right]E(z) = 0 \tag{9}$$

The closed-loop error dynamics are selected to allow the system to exhibit a first-order response. This is accomplished by making the second closed-loop pole at least one order of magnitude smaller than the dominant closed-loop pole. The dominant pole is selected from operator experience in order to decrease the settling time as much as possible without causing controller instability. Two over-damped poles are selected with time constants $\tau_1 = 1.5$ s and $\tau_2 = 0.15$ s. The desired closed-loop characteristic polynomial is

$$z^2 - 1.449z + 0.4806 = 0 \tag{10}$$

Equating the characteristic polynomials in equations (9) and (10), the controller polynomial coefficients are $g_1 = -0.549$ and $g_2 = 0.517$. The control signal is related to the reference and error signals by

$$v(z)b(z)U(z) = v(z)a(z)R(z) - g(z)E(z) \tag{11}$$

Equation (11) is expanded and transformed into a difference equation

$$U(i) = U(i-1) + \frac{1}{b_0}\left[R(i+1) + (a_0 - 1)R(i) - a_0 R(i-1) - g_1 E(i) - g_0 E(i-1)\right] \tag{12}$$

Equation (12) is coded into the Delta Tau language and implemented for controller validation. An experiment is conducted with a step reference input. Plots of the force measurements, reference, and control signal are shown in Figure 9. The controller allows

for robust tracking of a step reference with an approximate settling time of 5.5 s. To improve the response time the reference force is ramped at 70 N/s, 80 N/s, and 90 N/s to determine the ramp to decrease the settling time. The results, shown in Figure 10-12, demonstrate an approximate settling time of approximately 8 s, 7 s, and 6 s respectively and an average error of 0.26N, 0.18N, and 0.29N respectively. For subsequent experiments conducted with alumina, the reference forces have ramp trajectories with a slope of 80 N/s.

For the zirconium diboride paste, an experiment is conducted with a step reference force input initially. The settling time in this case is 5 s as seen in Figure 13. To improve the response time the reference force is ramped at 40 N/s, 50 N/s, and 60 N/s to determine the ramp to decrease the settling time. The results, shown in Figure 14 - Figure 16, demonstrate an approximate settling time of approximately 6 s, 4.5 s and 2.5 s respectively and an average error of 1.59 N, 0.56 N and 1.8 N respectively. For subsequent experiments conducted with zirconium diboride, the reference forces have ramp trajectories with a slope of 50 N/s.

5. Extrusion on Demand Approaches

5.1. Dwell Method

Two approaches for achieving EOD are investigated in this research. One method, called the dwell method, uses a dwell allowing the extrusion force to attain the required value to start extrusion and with ram retraction to stop extrusion. The other method, called the trajectory method, establishes a pre-deposition position trajectory and increases or decreases the force before the actual point of start or stop of deposited path is reached.

A diagram showing the nozzle movement path for the dwell method is shown in Figure 17a. Point A indicates the start of deposition and point B indicates the end of deposition. Extrusion on demand is achieved by dwelling at point A until the extrusion force reaches a certain percentage of the reference force. The nozzle begins its motion after this specified force is attained. The nozzle then moves to point B and dwells there, where the paste flow is stopped by creating a suction inside the syringe by retracting the ram at the maximum motor speed of 128 mm/s. This is achieved by terminating the gantry motion at B and retracting ram for three seconds prior to activation of the next motion command. If the stop dwell time is set to less than three seconds excess material is observed at the nozzle tip. For stop dwell times more than three seconds, the ram retracts further back than desired. To determine the start dwell as a function of the reference extrusion force, different ram forces as percentages of the reference extrusion force are tested. To fine-tune this method, different start dwell times are tested. For alumina, the extrusion force used is 450 N and deposition is performed at a standoff distance of 55% of the extrudate diameter. Results of the start dwell test, shown in Figure 18, consist of five 127 mm lines, which are extruded at dwells ranging from 50% to 70% in 5% increments of the reference force. Lines deposited with dwell times less than 65% are discontinuous due to the changing velocity profile at the beginning of each deposition as there is a delay in achieving steady state velocity. Also, the tapering is about 62% for the continuous portion of the deposition. The deposition is continuous when the dwell is 65% and 70% and the tapering of lines obtained is 44%-56% .Hence this range is used. For zirconium diboride, the extrusion force is set to 150 N and the standoff distance is 55% of the extrudate diameter for each test. Figure 19 shows the results of the various

dwells as percentage of reference extrusion force that are tested. It can be observed from the results of the dwell tests that for an extrusion force of 150 N, dwells between the ranges of 60% to 70% of extrusion force exhibit the least amount of taper (21%) compared to others of (45%). Dwells at 50% of extrusion force exhibit discontinuities at the beginning of the line. Hence, the dwells are bounded between 60% and 70% of required force.

5.2. Trajectory Method

Figure 17b illustrates the path of nozzle movement for the trajectory method. The line to be deposited is A-B. The distances are calculated using the time and velocity inputs. The controller switches on at point C at the start of deposition. Distance A-C is calculated using the extrusion velocity and start time inputs given. The appropriate time inputs are established via various experiments. During the stop movement point D is established where the controller switches to a low force (20N) before the actual end point of the trajectory at B. This ensures that the paste flow has stopped when the gantry reaches point B. Various start times and stop times are tested to tune the EOD method. Figure 20 shows the start time tests for alumina. It can be seen that the extrusion is delayed at the start due to insufficient start times of 3 s and 3.5 s. Excess material deposition is observed due to an excess start time of 4.5 s. Deposition starts at the expected point as indicated by the vertical line when start time is 4 s. Figure 21 shows the stop time tests conducted using alumina paste. The vertical line indicates the precise location of end of extrusion. A stop time of 0.7 s leads to an early stop of deposition. The deposition stops at the expected point when stop time 0.65 s. Excess material deposition

is observed when stop time is 0.6 s. Figure 22 shows the start time tests for zirconium diboride. Excess material deposition is observed with start time of 3.5 s and 3 s. Deposition starts at the expected point as indicated by the vertical line when start time is 2.5 s and 2 s. Extrusion is delayed at the start when start time is 1.5 s. Figure 23 shows the stop time tests conducted using zirconium diboride paste. A stop time of 0.65 s leads to an early stop of deposition. The deposition stops at the expected point when stop time 0.6 s. Excess material deposition is observed when stop time is 0.55 s.

Before every start and after every stop movement the gantry is commanded to move to a brush which cleans the nozzle tip to remove any excess material accumulation and prevents clogs. The nozzles used in this method have a longer die-land (37 mm) than the nozzles used in the dwell method (20 mm) to ensure that good continuous extrusion is obtained. This is because the dwell method relies on the speed of retraction of the paste back into the nozzle. Paste cannot be retracted fast enough through a longer die land as the length of paste travel is greater. Also, the presence of excessive paste in the die land before the start of extrusion results in excess material deposition at the beginning of every deposited line. The excess paste accumulated at the beginning of deposition results in the nozzle dragging through the excess paste, eventually clogging the nozzle. Hence, a longer die land cannot be used in the dwell method.

Both the above mentioned methods can be used to achieve EOD. The trajectory method ensures that the gantry is moving once steady state extrusion has been obtained. However, the occurrences of nozzle clogging are higher in this method due to a longer die land. The paste freezes in the longer die land quickly as compared to a shorter die land. Hence this method requires frequent stopping of the part fabrication process to clear

the die land. This is not advisable as it interferes with the part fabrication process. Also the trajectory method relies heavily on the efficiency of the tip cleaning process. The tip cleaning equipment is a simple brush in the current experimental set-up. Hence, the effectiveness of this cleaning method is not always guaranteed. In the dwell method the lines are deposited with an inherent taper. Material accumulation at the start occurs due to the dwell of the gantry and the thickness of the line being deposited increases gradually. The dwell tests performed for alumina and zirconium diboride pastes allow the selection of force-dwell combinations in which lines of most uniform thickness are obtained. Also the extrusion may not be at a steady state value when the gantry has started moving. Both the EOD methods result in similar quality of part build.

6. Process Parameters

Many process parameters affect the quality of the FEF process. This paper will analyze the effects of table velocity, standoff distance, dwell periods, overlap factor. The viscosity of the alumina paste is $280 \cdot 10^5$ cP at a shear rate of 101.893 s^{-1} with a shear exponent approximately 0.109 and that of zirconium diboride is $240 \cdot 10^5$ cP at a shear rate of 101.893 s^{-1} with a shear exponent approximately 0.131. The viscosity of the paste is measured using a Brookfield DV II viscometer. The shear exponents are calculated by measuring torque and revolutions of the mixer blades of a Brabender shear mixer (Hilmas and Beaff 2006). The shear rate is calculated from this data (Hilmas and Xu 2006). Plots of shear rate vs. torque are shown in Figure 24. The slope of this plot is the shear exponent. Working ranges for all the process parameters have been established through the experiments conducted. The environmental temperature and heating temperature have been fixed. The environmental temperature refers to the temperature of the freezer in

which the gantry system is contained. Liquid nitrogen is used to regulate the freezer temperature at -5 °C. The heating temperature refers to the temperature maintained by the heating tape around the sleeve of the stainless steel syringe. This value is fixed at 20 °C for this study. The nozzle diameter for all experiments in this paper is fixed at 580 µm.

6.1. Extrudate Diameter

Extrudate diameter is measured by photographing the extrudate during steady-state operation with a steel ruler placed next to the ram setup. The setup is shown in Figure 25. Pixels on one inch of the ruler are measured in the photograph. The pixels along the length of the image of the extrudate are measured next. Comparison between these two pixels is used to calculate the extrudate diameter in inches. The experiment is conducted with constant extrusion forces ranging from 350 to 500 N in increments of 25 N. The average extrudate diameter is calculated to be 617 µm for alumina and 610 µm for zirconium diboride. Figure 26 shows a plot comparing the extrudate diameters measured using alumina and zirconium diboride paste for the range of extrusion forces. It can be seen from the plot that the extrudate diameter remains the same for various forces for a given paste with a resolution of 2 µm.

6.2. Table Velocity

The table velocity is the gantry velocity magnitude in the direction of deposition. The extrudate velocity is defined as the paste velocity as it exits the nozzle, and is generally on the order of mm/s. For good extrusion, the table velocity should be set equal to the extrudate velocity to ensure that paste is distributed uniformly. Table velocities that are higher than the extrudate velocity will result in thin and sometimes incomplete deposition (voids), while lower table velocities result in excessive deposition per unit length, causing surface defects from the nozzle dragging through the excessive

deposition. Figure 27 shows the results of deposition with velocities that are too high or too low. For velocities that are lower than desired there is excess material accumulation as the extrudate velocity is higher than table velocity. This causes the nozzle to drag through the deposited material. For extrudate velocities higher than the desired velocity the extrusion is discontinuous.

The extrudate velocity is measured by recording extrusion with a camera for a period of 2 minutes during steady-state operation with a steel ruler placed next to the ram setup. The resolution is 0.5 mm/s. A series of tests are conducted at extrusion forces ranging from 350 to 500 N in increments of 25 N using alumina paste to measure the steady-state extrudate velocity. The order of the forces is randomized. A series of tests is conducted using zirconium diboride paste for forces ranging from 150 N to 500 N at increments of 50N. Eight data points are measured for each force. A linear model is assumed for the extrusion velocity profile.

$$v = a \cdot F + b \tag{13}$$

Data collected from the experiments are plotted compared to the model using a least square fit. Plots comparing the experimental and modeled data for alumina and zirconium diboride paste are shown in Figures 28 and 29 respectively. The correlation coefficient for the least squares fit for the experimental data conducted using the alumina paste is 0.973 and for the data obtained using zirconium diboride paste is 0.952. These values of correlation coefficient are very close to 1 indicating that the first order model is acceptable. The sum of square of error for alumina is 0.26 and for zirconium is 5.16.

6.3. Standoff Distance

Standoff distance refers to the distance between the nozzle tip and the top of the substrate or previous layer, and is expressed in this study as a percentage of the measured extrudate diameter.

A series of thin walled rectangles 25.4 x 35.56 mm in dimension are fabricated using alumina paste with a ram extrusion force of 450 N and a table velocity of 4.9 mm/s. The results are shown in Figures 30a-e. The examined standoff distances are 45%, 50%, 55%, 60%, and 65% of the extrudate diameter. The part fabricated at 45% has visible horizontal striations and is thicker than the other parts indicating that the nozzle digs into the previous layers. Also the nozzle clogs at the last layer due to the excess material accumulated around it. The discontinuity in the extrusion is visible on the last layer. The parts fabricated at 60% and 55% both appear to have good layer consistency. The standoff distance of 65% is too high and causes the part to collapse. The corners are curved inside indicating that the nozzle does not flatten out the deposited line as it travels. The established range of standoff distances is bounded between 60% and 55%.

A series of thin walled rectangles, 25.4 x 35.56 mm, are fabricated using zirconium diboride paste with a ram extrusion force of 150 N and a table velocity of 5.3 mm/s. The results are shown in Figures 31a-e. The tested standoff distances are 45%, 50%, 55%, 60% and 65% of the extrudate diameter, respectively. The standoff distance of 45% is too low. The nozzle progressively digs into the previous layers, causing the part to collapse. The standoff distance of 65% is too high and causes the part to collapse. Parts fabricated with a standoff distance of 50%, 55% and 60% do not collapse and are not deformed. Therefore, the established range of standoff distances is bounded between 50% and 60% for zirconium diboride.

6.4. Overlap Factor

The overlap factor (K_{OL}) refers to the spacing between adjacent parallel lines deposited on the same layer and is defined as

$$K_{OL} = \frac{-d_{gap}}{D_{ext}} \tag{14}$$

where D_{ext} is the extrudate diameter and d_{gap} is the gap between deposited lines. An overlap factor of zero implies the distance between the centers of adjacent lines is exactly D_{ext} apart. Figure 32a-c illustrates the zero, negative and positive overlap factors. A positive overlap factor implies the distance between the centers of adjacent lines is less than the extrudate diameter, which can lead to accumulation of material and undesirable part quality. Negative overlap factor implies the distance between the centers of adjacent lines is greater than the extrudate diameter. Parts with excessive negative overlap factor have gaps between extruded lines, which lead to poor structural density and will ultimately lead to part collapse.

A series of single-track rectangles, 25.4 x 35.56 mm, are fabricated at a standoff distance of 55% of the extrudate diameter to determine the working range of overlap factors for both ceramic pastes. All tested values of overlap factor are negative due to the inherent compaction of deposited material caused by the standoff distance being less than the extrudate diameter. The results are shown in Figures 33a-g. For alumina, the values tested are -30%, -35%, -40%, -45%, -50%, -55%, and -60% with three cross-sections fabricated per overlap factor. Parts created at -30% and -35% overlap contain slight accumulation of material between deposited lines, implying the spacing is too close. Rastered parts at -60% overlap contain gaps between adjacent lines. Overlap factors of -

40% to -50% exhibit acceptable deposition quality, thereby bounding the process parameter between these values for alumina.

For zirconium diboride, the overlap factors tested are -45%, -50%, -55%, -60% and -65%. The results are shown in Figure 34a-e. Rastered parts at -65% contain gaps between adjacent lines. Rastered parts at -45% contain excessive material accumulation as the adjacent lines are placed too close together. Overlap factors of -50%, -55% and -60% create a smoother surface with no gaps or material accumulation.

7. Part Fabrication

This section presents experiments conducted to fabricate two dimensional cross-sections and three dimensional parts using both ceramic pastes. Table 1 lists all the process parameters used for part fabrication.

Table 1: Process parameters used in part fabrication

Parameter	Alumina	Zirconium Diboride
Viscosity (cP)	280×10^5	240×10^5
Shear Rate (s^{-1})	101.893	101.893
Shear Exponent	0.109	0.131
Extrudate Diameter (μm)	617	610
Extrusion/Table velocity (mm/s)	4.9	5.3
Extrusion Force (N)	450	150
Standoff Distance (%)	55	55
Overlap Factor (%)	-45	-55
Start Dwell (Dwell Method) (%)	65	60
Stop Dwell (Dwell Method) (s)	3	3
Start Time (Trajectory Method) (s)	4	2
Stop Time (Trajectory Method) (s)	0.65	0.60

The software Insight 4.3.1 is used to slice .stl files into sections and extrapolate extrusion paths based on the selected process parameters. The layer and tool path

generation process of a simplified fuel injector strut is shown in Figure 35. The part is scaled to 7.62 x 50.8 x 25.4 mm and oriented so that the larger dimensions are on the x-y plane, ensuring the build height is minimized.

The 74-layer simplified fuel injector strut fabricated using alumina is shown in Figure 36. One of the corners contains excess material due to the beginning of each deposition. The sides of the part exhibit a slight tapering indicating material accumulation due to the dwell method used. Figure 36c shows the simplified fuel injector part after post processes of vacuum freeze drying, binder burnout and pressureless sintering at 1550 °C.

Figure 37 shows the parts with a through hole fabricated using alumina paste with the trajectory method. The part's dimensions are 30.48 mm x 10 mm x 18mm in. It can be seen that the starts and stops at the outer contour for most layers are not uniform. However, the start and stop obtained for the rastering section is excellent.

Figure 38 shows a green part and a sintered part fabricated with an internal hole fabricated using zirconium diboride with the EOD dwell method. The dimensions of the green part are 30.48 mm x 10 mm x 5mm. The dimensions of the sintered part are 25 mm x 8 mm x 3 mm. The sintering shrinkage observed is 17% in length, 21% in width and 40% in height. The internal hole dimensions are 5mm in green part and 3mm in sintered part. The internal hole exhibits shrinkage of 40% in diameter.

Figure 39 shows a green part and a sintered part fabricated with an internal hole fabricated using zirconium diboride with the EOD trajectory method. The sintering shrinkage observed is 17% in length, 21% in width and 40% in height. The dimensions of the sintered part are 25 mm x 8 mm x 3 mm. The internal hole dimensions are 5mm in

green part and 3mm in sintered part. The internal hole exhibits shrinkage of 40% in diameter.

7.1 Post Processing Schedules and Results

7.1.1 Freeze Drying

For alumina, the temperature is at -16°C for 2-5 days depending on sample size. For zirconium diboride, the schedule is shown in Figure 41.

7.1.2 Binder Burnout

For alumina, the samples are heated to 600°C at 1°C/min, held at 600°C for 1 hour and then cooled to room temperature. For zirconium diboride, the samples are heated to 600°C at 0.5 °C/min, held at 600°C for 1 hour and then cooled to room temperature.

7.1.3 Pressureless Sintering

For alumina, parts are sintered at 1550 °C at 0.5 °C/min. For zirconium diboride, a three stage sintering schedule is followed. A graphite furnace is used for this purpose. First, the parts are heated to 1350°C at 10°C/min and held for 1 hour in vacuum. This is followed by heating to1500°C at 10°C/min and samples are held for 1 hour in vacuum. The furnace is flowed with argon and samples are heated to 2100°C at 25°C/min and samples are held for 2 hour with flowing argon. The samples are then cooled to room temperature at 25°C/min.

Table 2 shows the sintered density measurements of 5 zirconium diboride samples. The densities are measured using Archimedes Principle (Huang T.S. 2007).

Table 2: Density measurements of 5 zirconium diboride samples.

Sample	Dry Wt. (D) (g)	Saturated Wt. (St) (g)	Suspended Wt. (Su) (g)	Density= D/(St-Su)*density of water (g/cc)	Theoretical Density (g/cc)	Relative Density (%)
1	2.7854	2.8824	2.346	5.2	5.67	92
2	1.71	1.7271	1.4164	5.503	5.67	97
3	1.0464	1.0565	0.8523	5.12	5.67	90
4	1.1306	1.1632	0.946	5.2302	5.67	92
5	0.9127	0.9291	0.7553	5.303	5.67	93

The high densities are obtained due to addition of sintering additives like boron carbide and carbon black.

8. Summary

Extrusion on Demand for ceramics using Freeze-form-Fabrication has been discussed in this paper. The combined implementation of a general tracking controller with integral action and adjustment of deposition dwell times was used. Step tests were implemented to establish a first-order model. The established model was used to design the general tracking controller for regulating the extrusion force. Experiments were conducted to measure extrudate diameter and extrusion velocity for alumina and zirconium diboride pastes for a variety of extrusion forces. Experiments were conducted to establish the working ranges of table velocity, standoff distance, dwell time, start time

and overlap factor. These experiments were conducted using alumina and zirconium diboride pastes. Three-dimensional parts were fabricated using the two EOD methods with alumina and zirconium diboride. The EOD methods used were the dwell method and the trajectory method. The dwell method uses start and stop dwells allowing the extrusion force to attain the required value to start or stop extrusion. The trajectory method establishes a pre-deposition position trajectory and increases or decreases the force before actual point of start or stop of deposited path is reached. The green parts were subjected to post processes and densities of the sintered parts were measured.

9. Conclusions

The extrusion force process can be modeled as a first order dynamic system. The controller is capable of achieving a faster response with a ramp input compared to a step input. The extrudate diameter is constant for all forces for a particular nozzle size. The standoff distance required for good part fabrication is lower than the track height. Negative overlap factors have to be used in part fabrication process as the paste spreads out during deposition to obtain the required cross section. Table velocities and extrusion velocities have to be equal for obtaining continuous deposition. The least squares fit for the data relating extrusion force to extrusion velocity for both pastes has a value of R close to 1 indicating a good model. The sum of square of the error is 0.26 for alumina and 5.16 for zirconium diboride. The required start dwell period and start times are dependent on the measured force. Any values outside the working ranges for process parameters lead to part collapse. Two dimensional cross sections and solid parts with holes prove that internal features and parts with complex geometries can be fabricated using EOD in FEF. The time constant for alumina paste is greater compared to zirconium diboride paste

as it is more viscous. The difference in the viscosities and shear exponents also explains the gain for alumina being lower than the gain for zirconium diboride i.e. more force is required to obtain same velocities. Difference in viscosity explains the use of lower extrusion force, higher extrusion velocity, different start times, dwells and overlap factors for zirconium diboride paste compared to alumina.

10. Acknowledgments

The authors wish to acknowledge the financial support for this work from the Missouri S&T Center for Aerospace Manufacturing Technologies (Air Force Research Laboratory contract FA8650–04–C–5704) and the Missouri S&T Intelligent Systems Center.

11. References

1. Agarwala, M.K., Bandopadhyay, A., Weeren, R., Safari, A., Danforth, S.C., Langrana, N.A., Jamalabad, V., and Whalen, P.J., 1996, FDC, Rapid Fabrication of Structural Components, The American Ceramic Society Bulletin, Vol. 65, pp. 60-65.

2. Amarasinghe, A.D.U.S. and Wilson, D.I., 1998, Interpretation of Paste Extrusion Data, Chemical Engineering Research and Design, Vol.76, No. (A1), pp. 3-8.

3. Bellini, A., 2002, Fused Deposition of Ceramics: A Comprehensive Experimental, Analytical and Computational Study of Material Behavior, Fabrication Process and Equipment Design, PhD Dissertation, Drexel University, Department of Mechanical Engineering.

4. Benbow, J.J., and Bridgewater, J., 1992, Paste Flow and Extrusion, Clarendon Press, Oxford.

5. Calvert, P., Lombardi, J., Mulligan, A., and Stuffle, K., 1993, Solid Freebody Forming from Polymerizable Slurry, Proceedings of Solid Freeform Fabrication Symposium, Austin, Texas, pp. 60-63.

6. Cesarano, J., King, B., and Denham, H.B., 2004, Recent Developments in Robocasting of Ceramics and Multimaterial Deposition, Proceedings of Solid Freeform Fabrication Symposium, Austin, Texas, pp. 679-703.

7. Hilmas, G.E., Xu, X., 2007, The Rheological Behavior of Ceramic/Polymer Mixtures for Coextrusion Processing, Journal of Materials Science, Vol. 42, pp. 1381 -1387.

8. Hilmas, G.E., Beeaff D.R., 2002, Rheological behavior of coextruded multilayer architectures, Journal of Materials Science, Vol. 37, pp. 1259 -1264.

9. Huang, T.S., 2007, Fabrication of Ceramic Components Using Freeze-Form Extrusion Fabrication, PhD Dissertation, University of Missouri, Rolla, Ceramic Engineering.

10. Huang, T.S., Mason, M.S., Hilmas, G.E., and Leu, M.C., 2006, Freeze-form Extrusion Fabrication of Ceramics, Virtual and Physical Prototyping, Vol. 1 (2), pp. 93-100.

11. Mason, M.S., Huang, T., Leu, M.C., Landers, R.G., and Hilmas, G.E., 2007, Aqueous–Based Extrusion Fabrication of Ceramics on Demand, Solid Freeform Fabrication Symposium Proceedings, Austin, Texas, pp.124-134.

12. Wang, J. and Shaw, L., 2005, Rheological and Extrusion Behavior of Dental Porcelain Slurries for Rapid Prototyping Applications, Materials Science and Engineering A, Vol. 397, No.1-2, pp. 314-321.

13. Xiong, Z., Yan, Y., Wang, S., Zhang, R., and Zhang, C., 2002, Fabrication of Porous Scaffolds for Bone Tissue Engineering via Low Temperature Deposition, Scripta Materialia, Vol. 46, No. 11, pp. 771-776.

14. Yang, S., Yang, H., and Evans J.R.G., 2006, Direct Extrusion FreeForming of Ceramic Pastes, Solid Freeform Fabrication Symposium Proceedings, Austin, Texas, pp. 304-315.

15. Yang, S., Yang, H., Evans, J.R.G., Chi., X, Thompson, I., Cook, R.J. and Robinson, P., 2008, Rapid Prototyping of Ceramic Lattices for Hard Tissue Scaffolds, Materials and Design, Vol. 29, pp.1802-1809.

16. Zhao, X., Landers, R.G., and Leu, M.C., 2008, Adaptive Control of Freeze–form Extrusion Fabrication Processes, ASME Dynamic Systems and Controls Conference, Ann Arbor, Michigan.

17. Zhao, X., Mason, M.S., Huang, T.S., Leu, M.C., Landers, R.G., Hilmas, G.E., Easley, S.J., and Hayes, M.W., 2007, Experimental Investigation of Effect of Environment Temperature on Free-form Extrusion Fabrication, Solid Freeform Fabrication Symposium Proceedings, Austin, Texas, pp. 135-146.

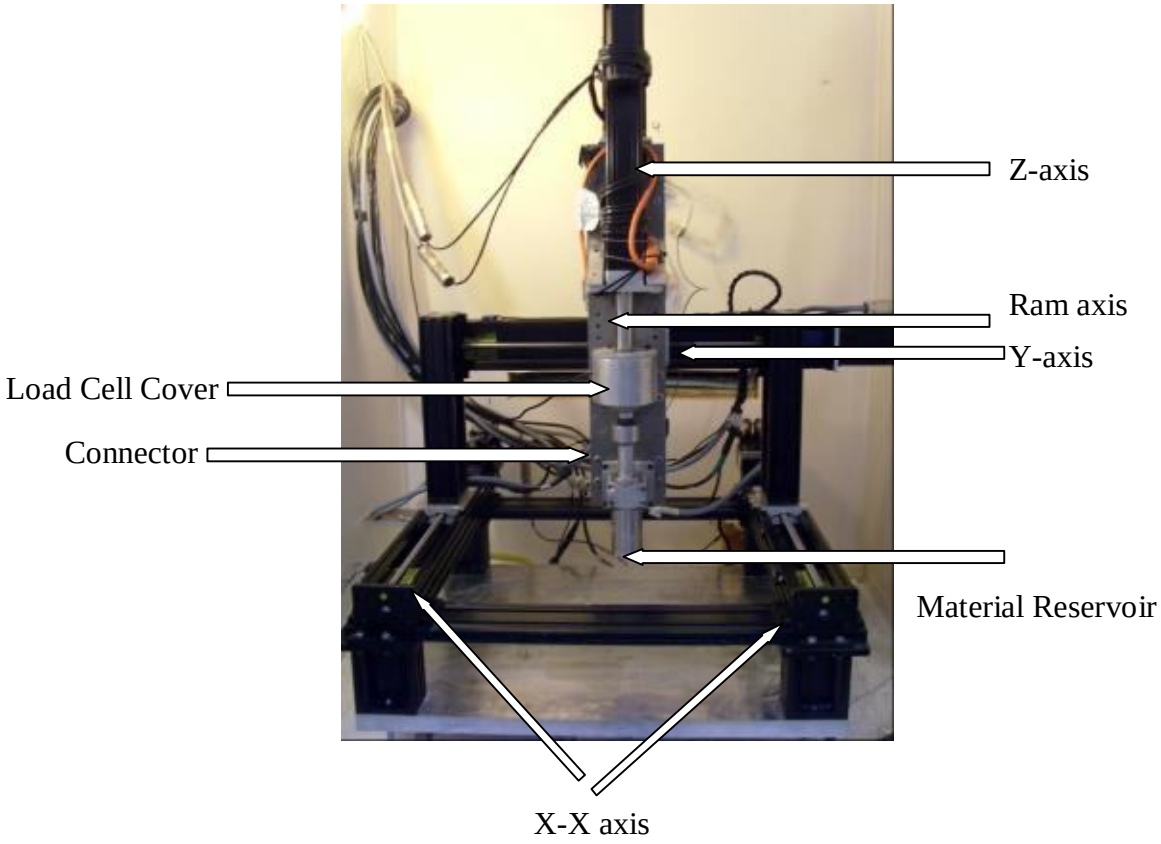

Figure 1: Freeze-form Extrusion Fabrication System.

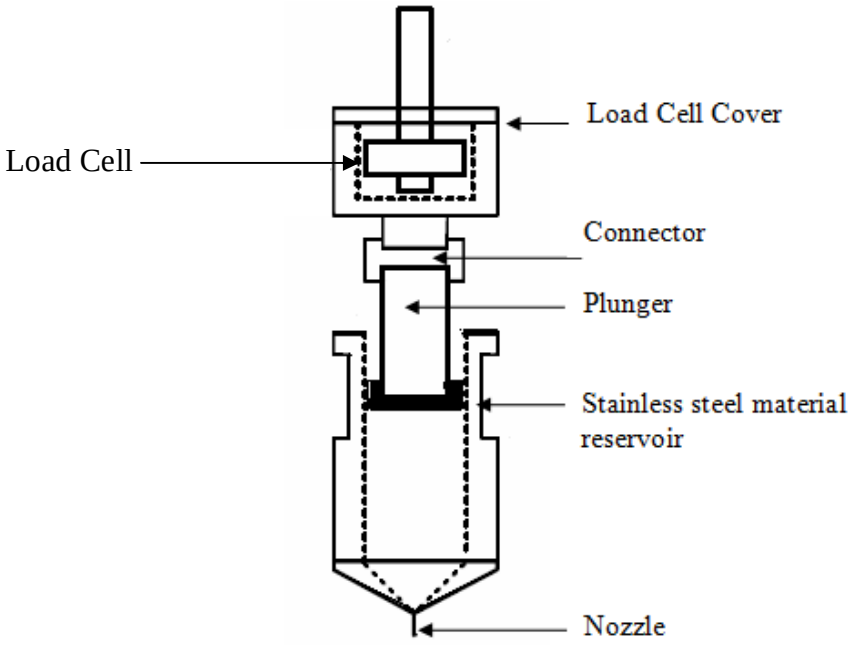

Figure 2: Ram Extruder Setup Schematic.

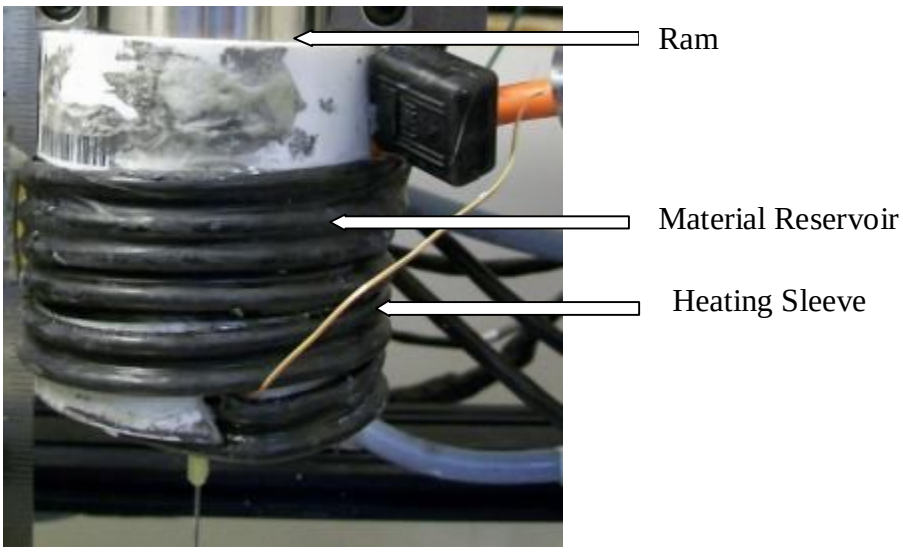

Figure 3: Heating Sleeve Assembly.

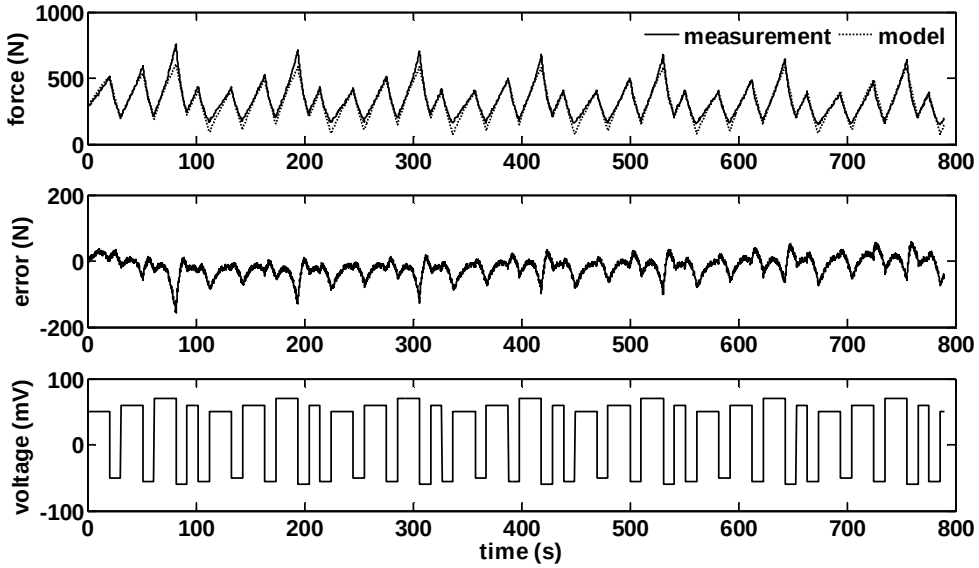

Figure 4: Input, Experimental Response, and Model Response for Model Parameter Identification Experiment for Alumina Paste.

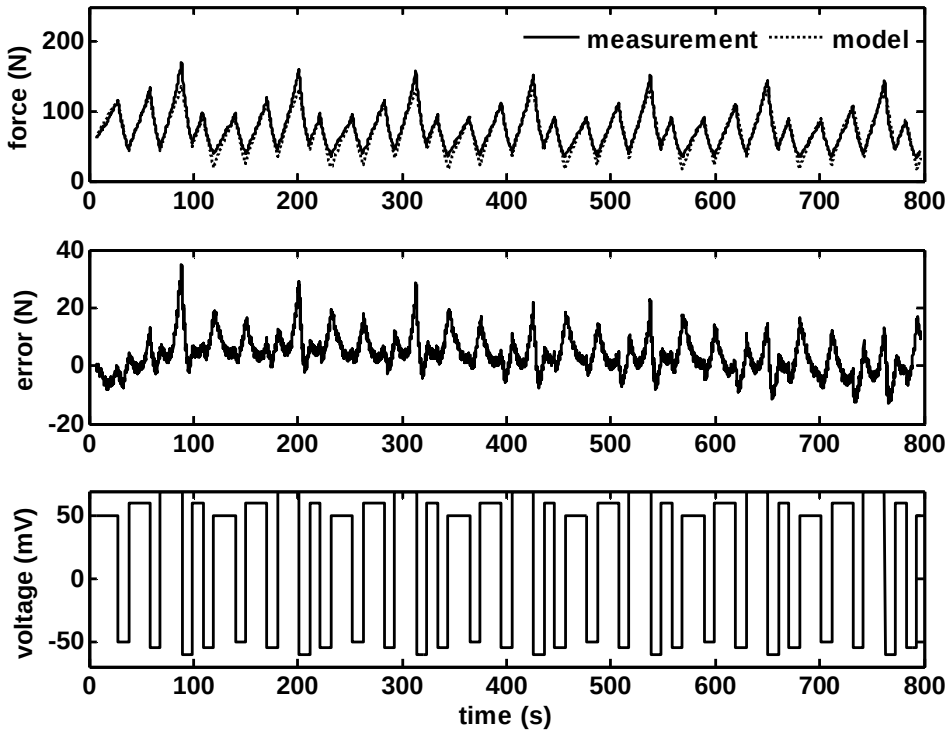

Figure 5: Input, Experimental Response, and Model Response for Model Parameter Identification Experiment for Zirconium Diboride Paste.

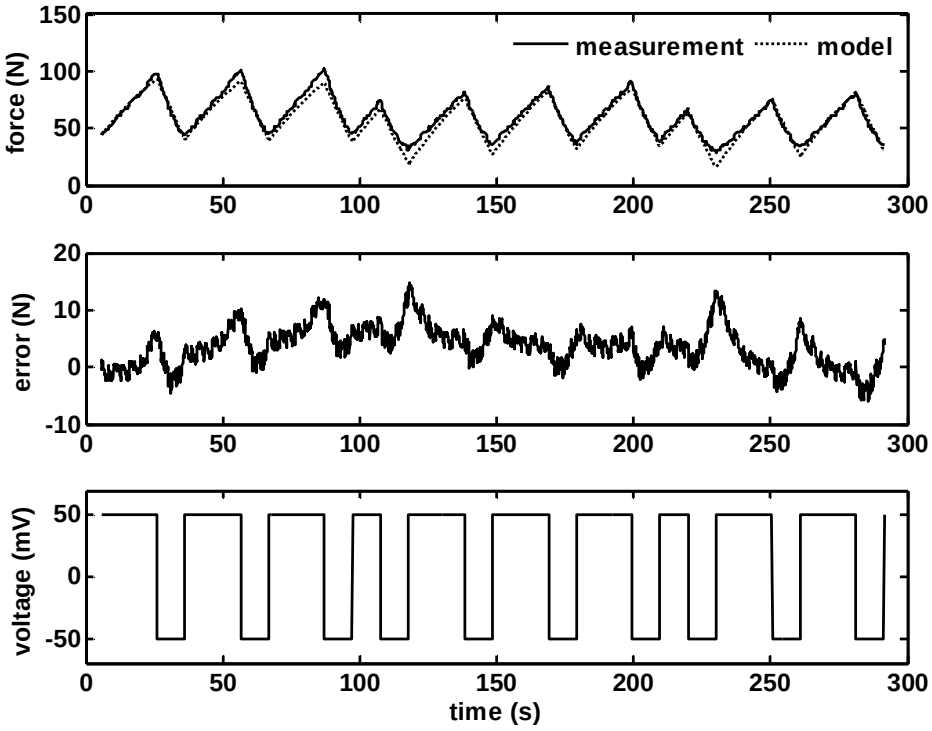

Figure 6: Input, Experimental Response and Model Response for Model Validation Experiment for Alumina Paste.

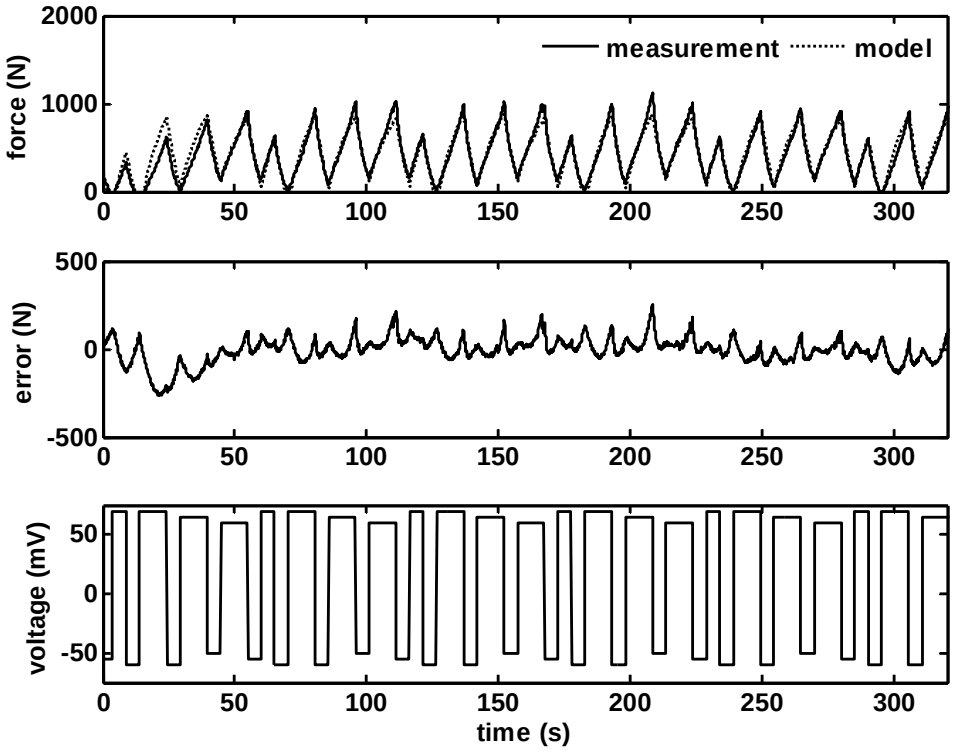

Figure 7: Input, Experimental Response and Model Response for Model Validation Experiment for Zirconium Diboride Paste.

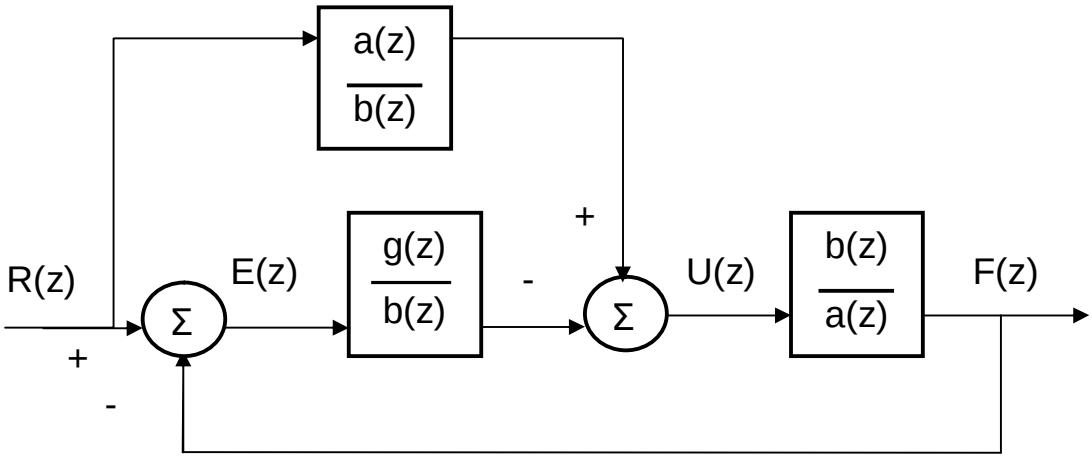

Figure 8: General Tracking Controller Block Diagram.

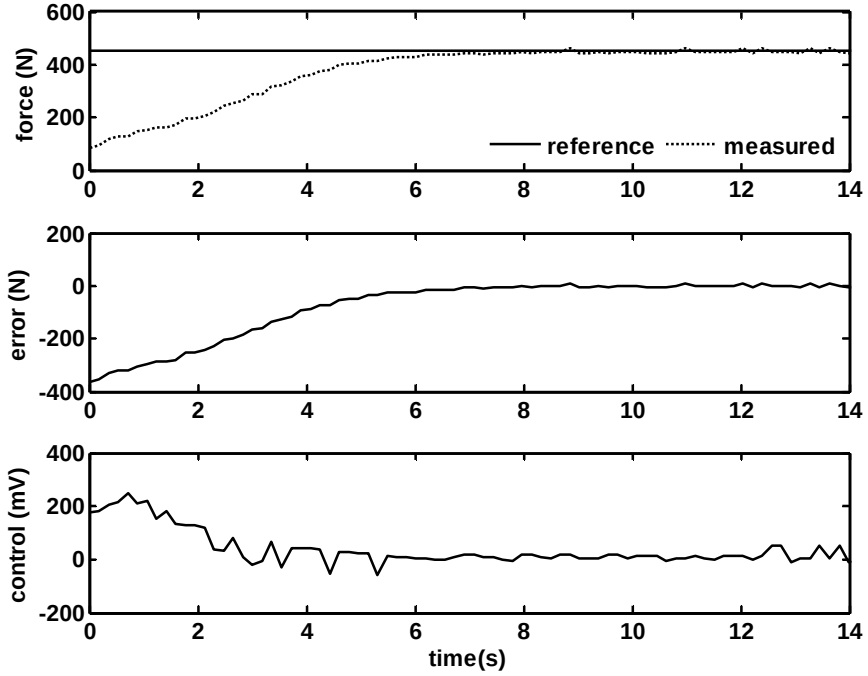

Figure 9: Extrusion Force Response to a Step Reference Extrusion Force (Alumina).

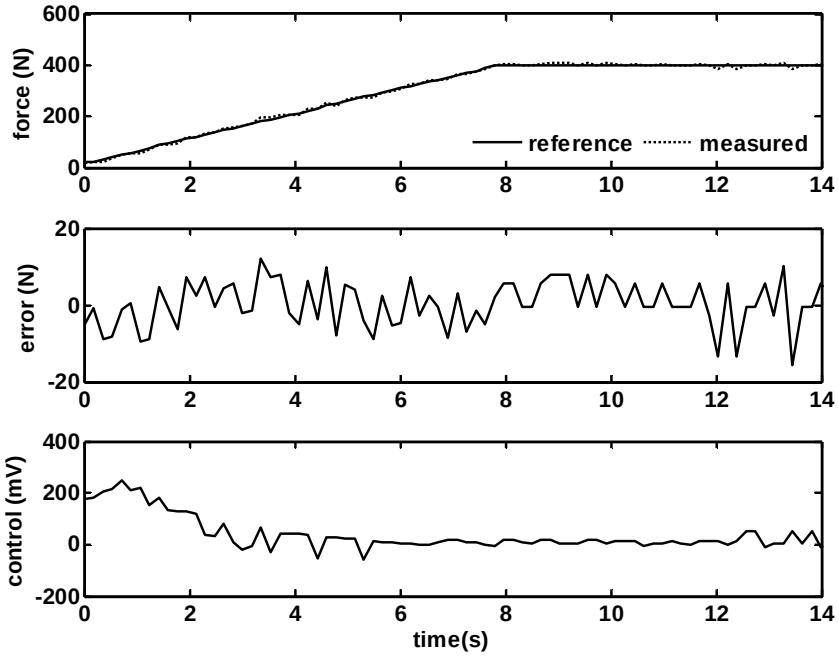

Figure 10: Extrusion Force Response to Reference Extrusion Force Ramped at 70N/s (Alumina).

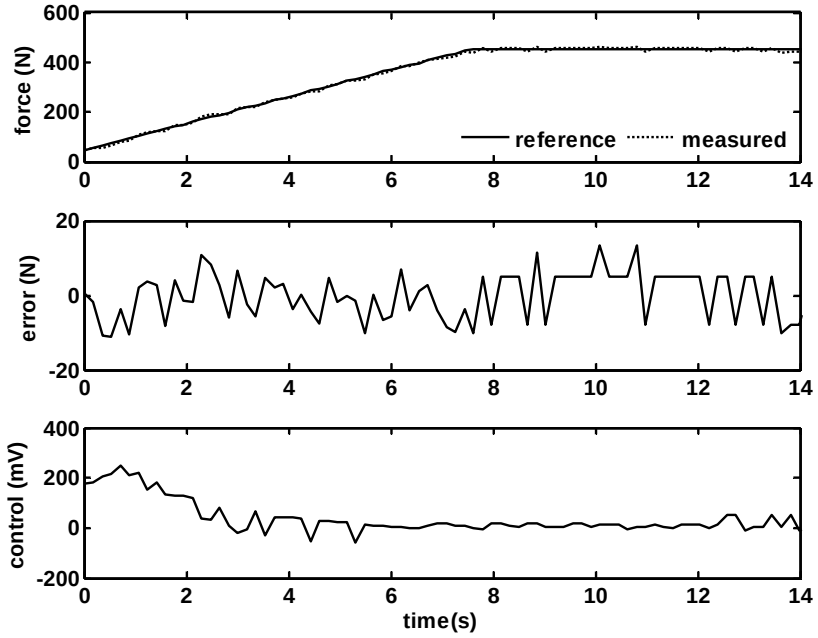

Figure 11: Extrusion Force Response to Reference Extrusion Force Ramped at 80N/s (Alumina).

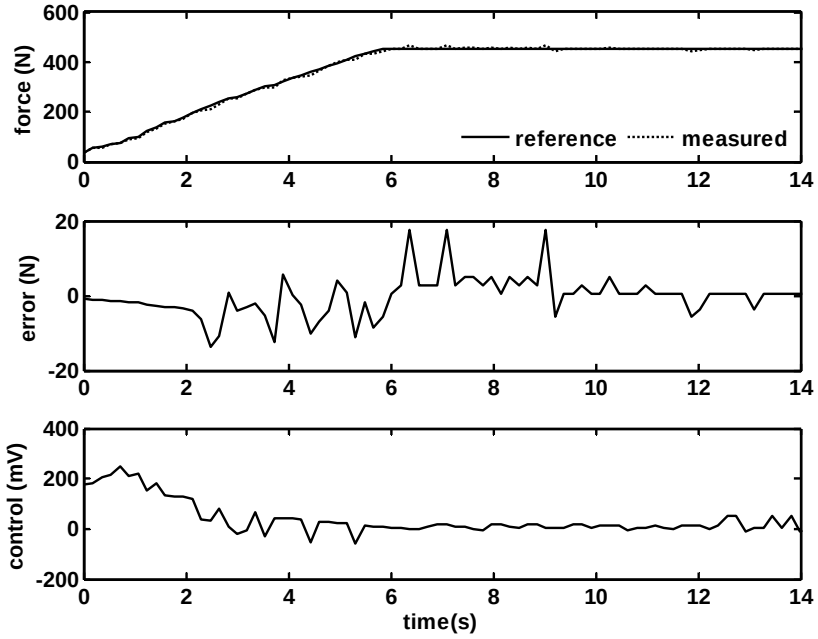

Figure 12: Extrusion Force Response to Reference Extrusion Force Ramped at 90N/s (Alumina).

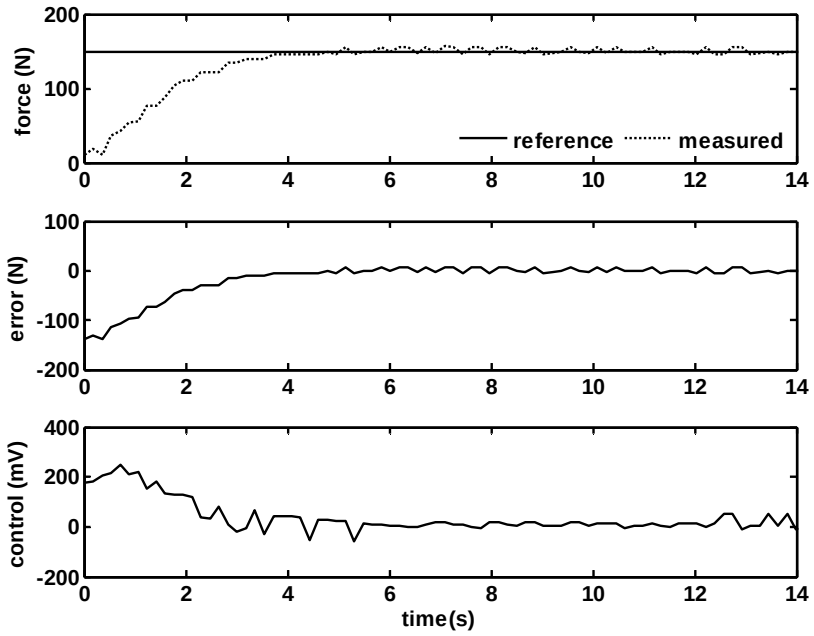

Figure 13: Extrusion Force Response to a Step Reference Extrusion Force (Zirconium Diboride).

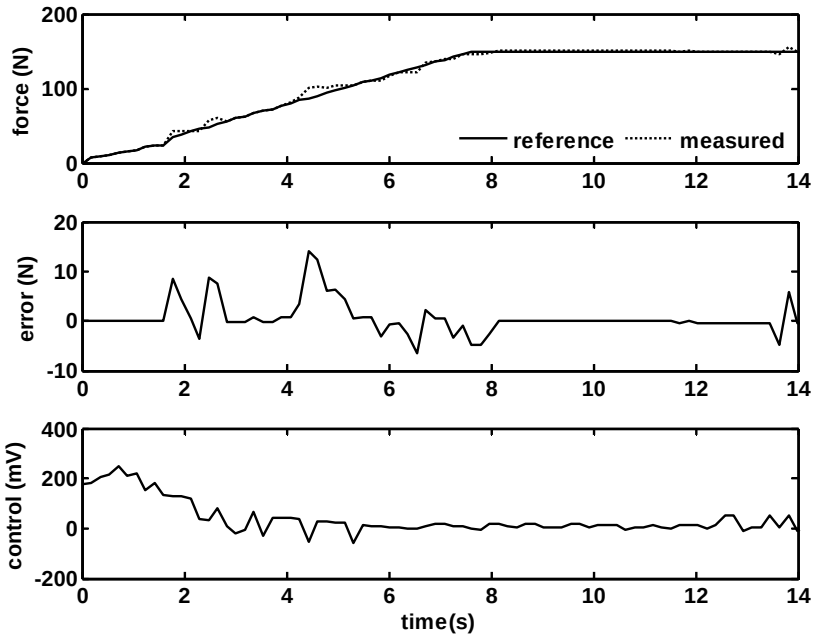

Figure 14: Extrusion Force Response to Reference Extrusion Force Ramped at 40N/s (Zirconium Diboride).

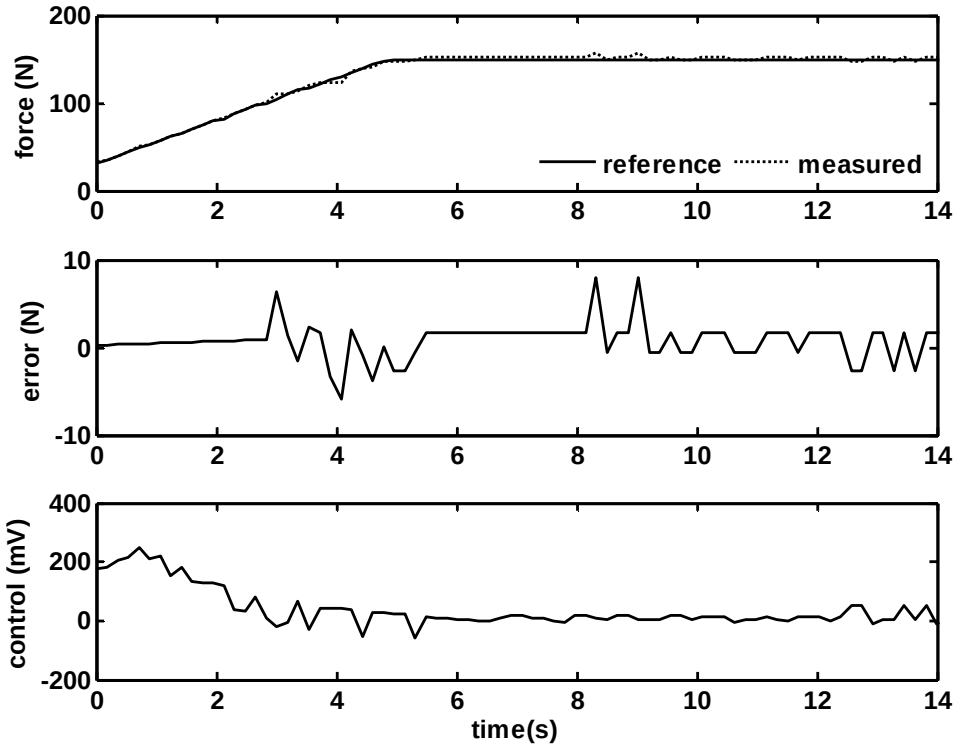

Figure 15: Extrusion Force Response to Reference Extrusion Force Ramped at 50N/s (Zirconium Diboride).

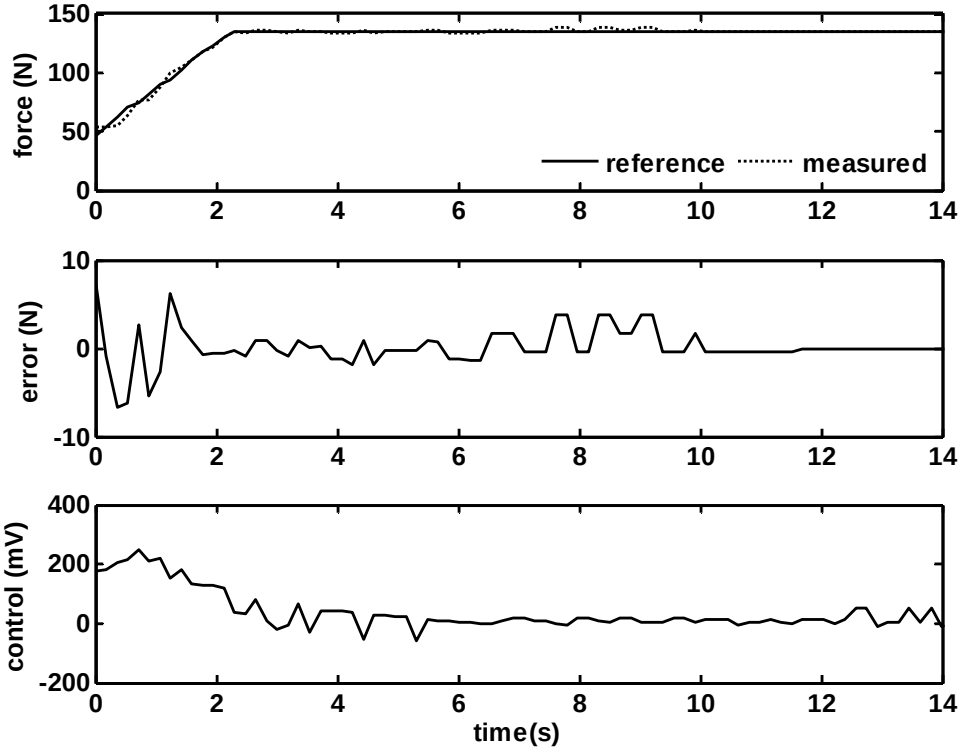

Figure 16: Extrusion Force Response to Reference Extrusion Force Ramped at 60N/s (Zirconium Diboride).

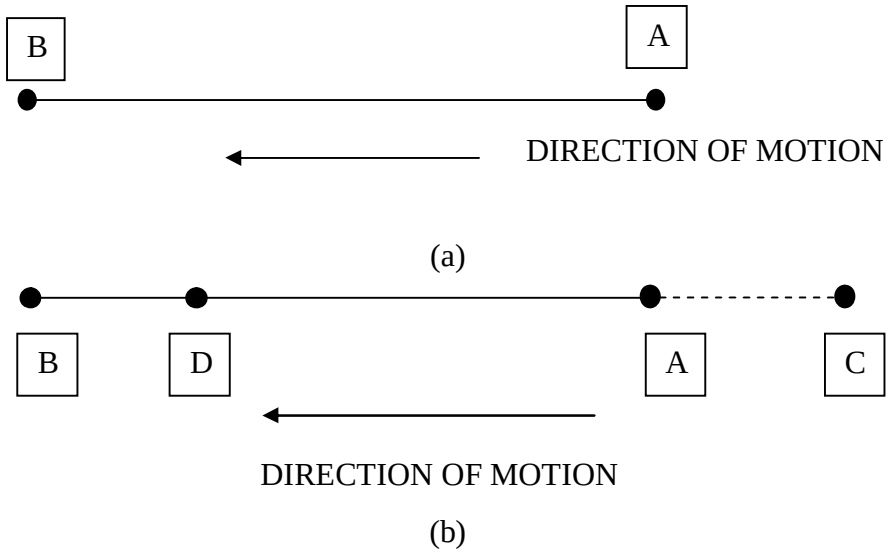

Figure 17: Schematic of Nozzle Movement for (a) Dwell Method (b) Trajectory Method.

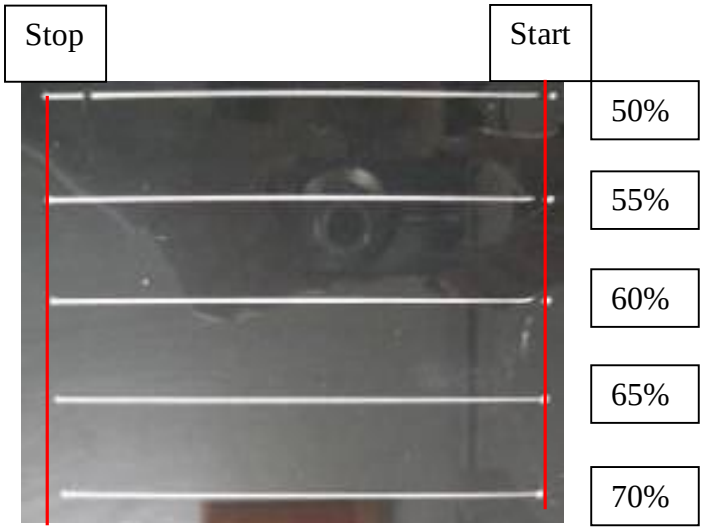

Figure 18: Deposited lines with dwells of 50%, 55%, 60%, 65% and 70% of extrusion force showing results of dwell tests conducted with Alumina Paste at 450 N. Standoff Distance is 55%. Table velocity is 4.9 mm/s. EOD dwell method is used.

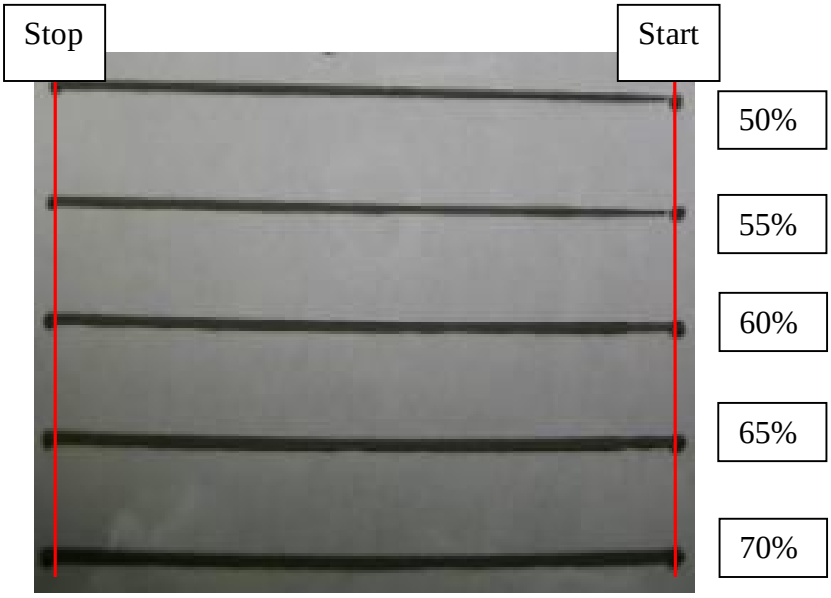

Figure 19: Deposited lines with dwells of 50%, 55%, 60%, 65% and 70% showing results of dwell tests conducted with Zirconium Diboride Paste at 150 N. Standoff Distance is 55%. Table Velocity is 5.3 mm/s. EOD Dwell method is used.

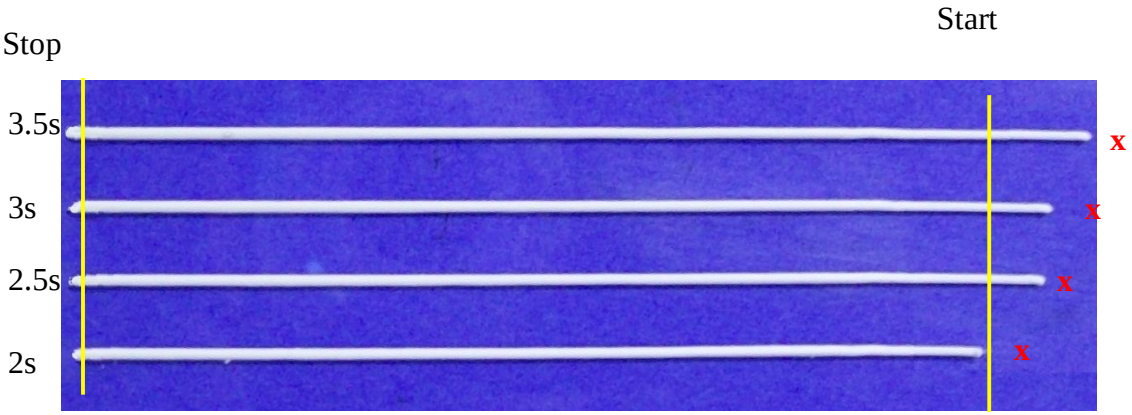

Figure 20: Start time tests for trajectory Method Conducted with Alumina paste at Times of 3.5 s, 3.0 s, 2.5 s and 2.0 s. Standoff Distance is 55%. Extrusion Force is 450 N. Table Velocity is 4.9 mm/s. 'x' Controller On.

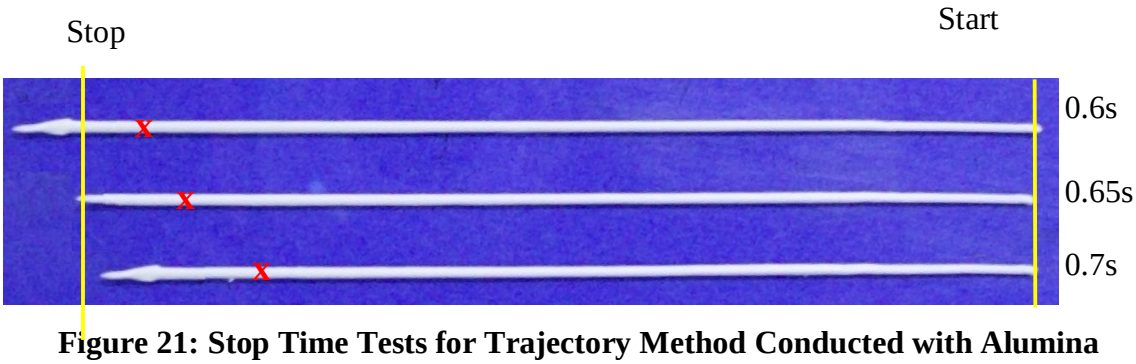

Figure 21: Stop Time Tests for Trajectory Method Conducted with Alumina Paste at Times of 0.7 s, 0.65 s and 0.6 s. Extrusion Force is 450 N. Table Velocity is 4.9 mm/s. Standoff Distance is 55% of Extrudate Diameter. 'x' Controller Off.

Figure 22: Start Time Tests for Trajectory Method Conducted with Zirconium Diboride Paste at Times of (a) 3.5 s, (b) 3.0 s, (c) 2.5 s, (d) 2.0 s and (e) 1.5 s. Standoff Distance is 55%. Extrusion Force is 150 N. Table Velocity is 5.3 mm/s.EOD Trajectory Method. 'x' Controller On.

Figure 23 : Stop time tests for trajectory Method Conducted with Zirconium Diboride paste at Times of 0.55 s, 0.6 s and 0.65 s. Extrusion force 150 N. Table Velocity 5.3 mm/s. Standoff Distance is 55% of Extrudate Diameter. 'x' Controller Off.

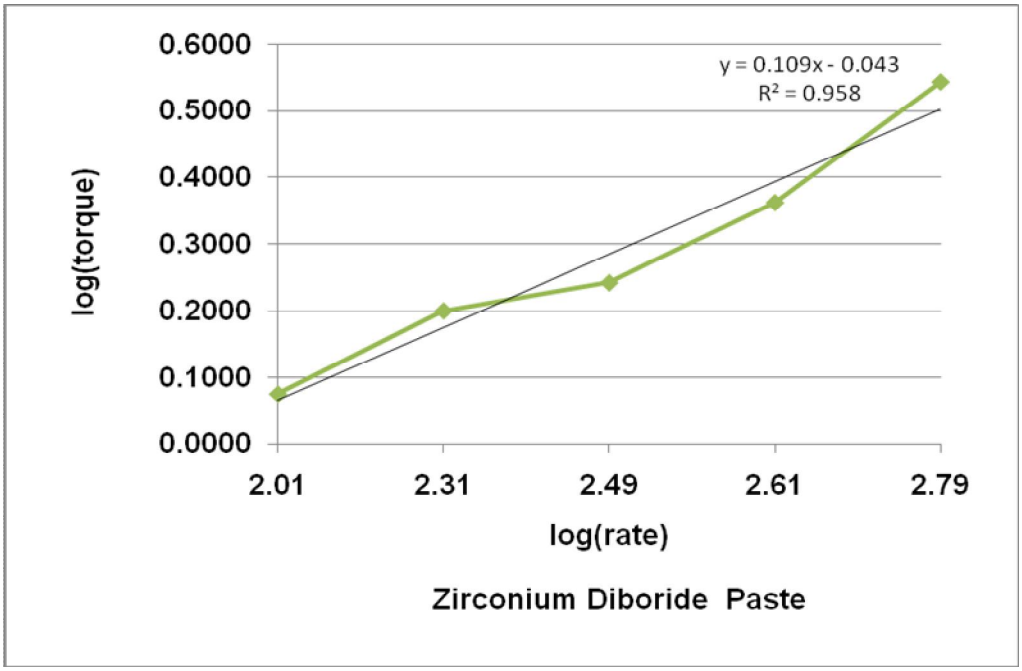

(a)

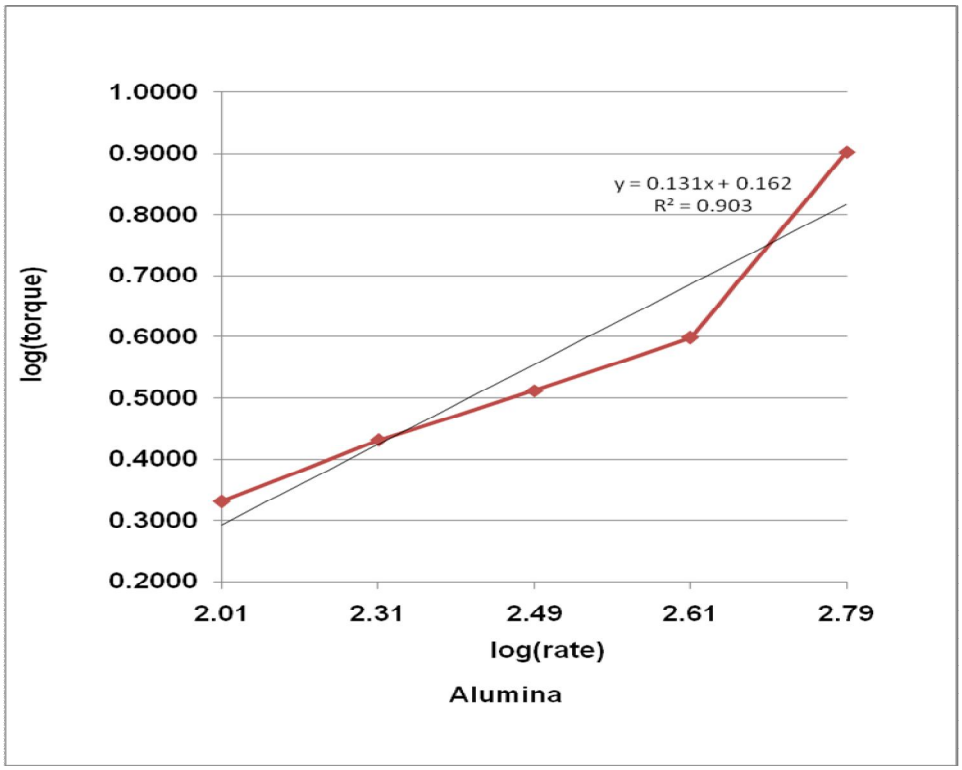

(b)

Figure 24: Graph of log (torque) vs. log (rate) for (a) Alumina Paste and (b) Zirconium Diboride Paste.

(a)

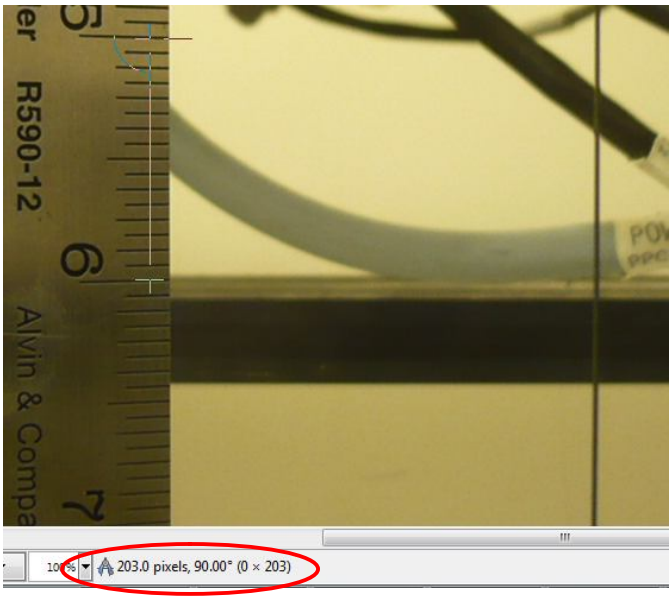

(b)

Figure 25: Pixel Comparison Method for Extrudate Diameter and Extrudate Velocity Measurement.(a) Set-Up (b) Pixels on One Inch of Ruler (c) Pixels on Actual Extrudate

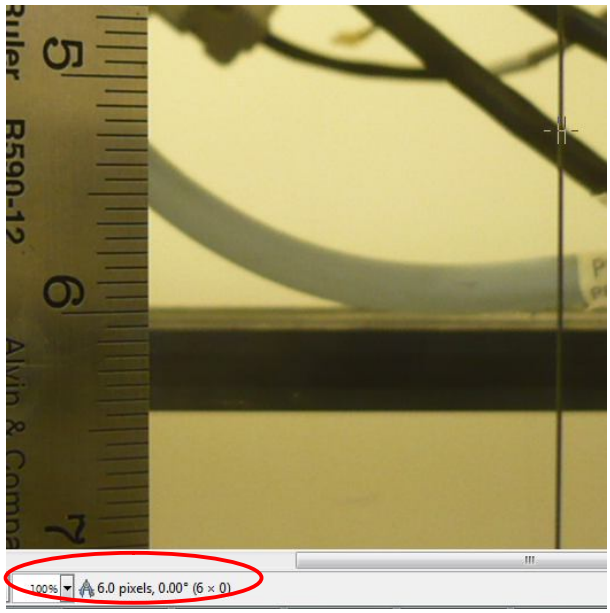

(c)

Figure 25(cont.): Pixel Comparison Method for Extrudate Diameter and Extrudate Velocity Measurement.(a) Set-Up (b) Pixels on One Inch of Ruler (c) Pixels on Actual Extrudate

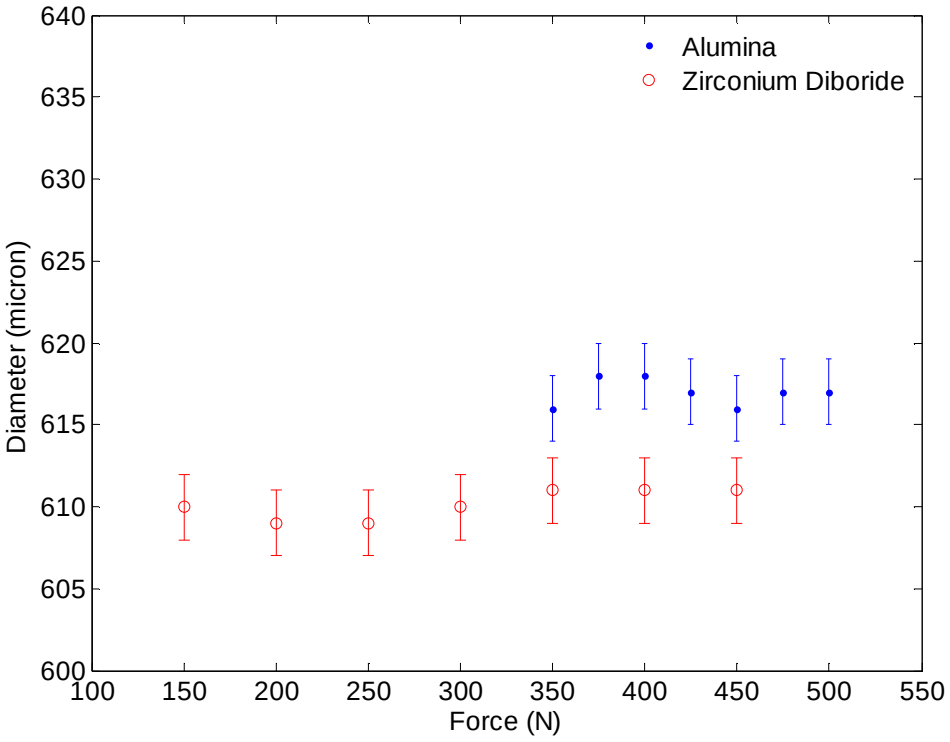

Figure 26: Extrudate Diameter Measurement, Nozzle Diameter = 580 µm.

(a)

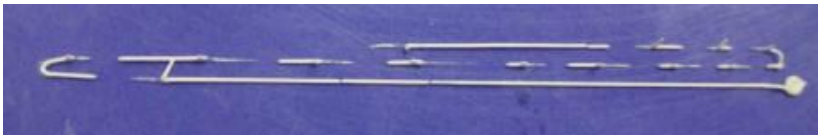

(b)

Figure 27: Excess and Discontinuous Extrusion Observed When Table Velocity is (a) Too Slow and (b) Too Fast. Alumina paste is used. Extrusion force is 450 N. EOD Dwell Method is used. Standoff Distance is 55%.

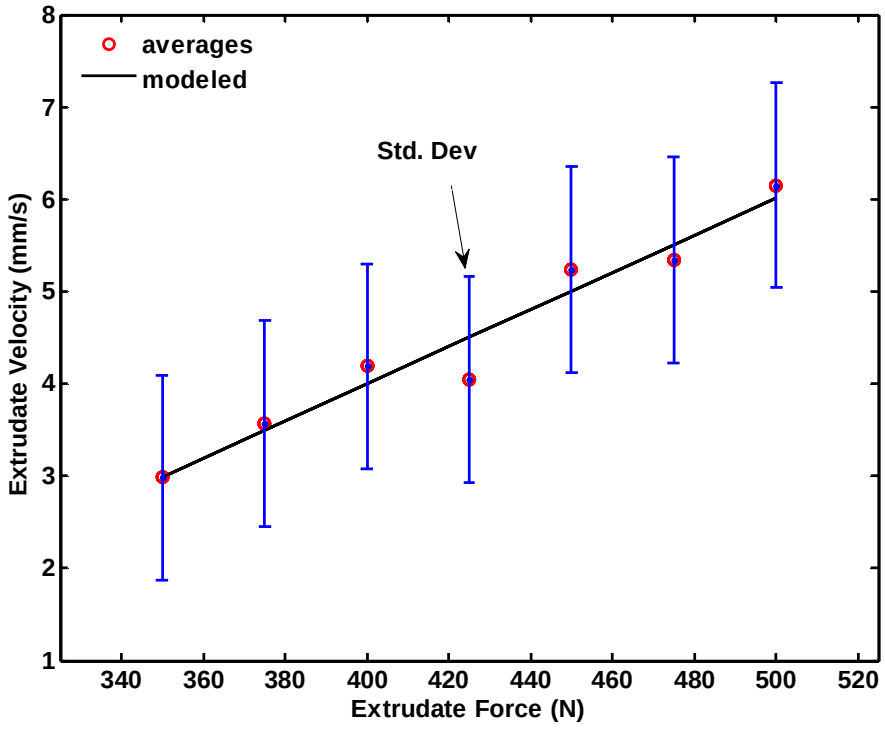

Figure 28: Plot Showing Least Squares Fit for Experimental and Modeled Extrusion Velocity Data (Alumina Paste).

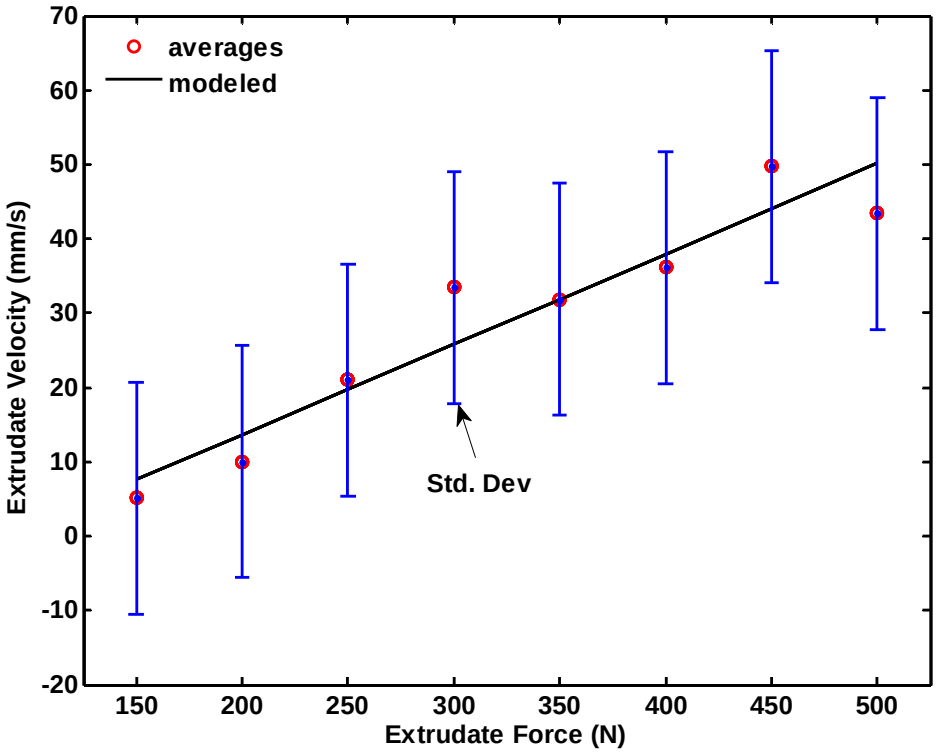

Figure 29: Plot Showing Least Squares Fit for Experimental and Modeled Extrusion Velocity Data (Zirconium Diboride Paste).

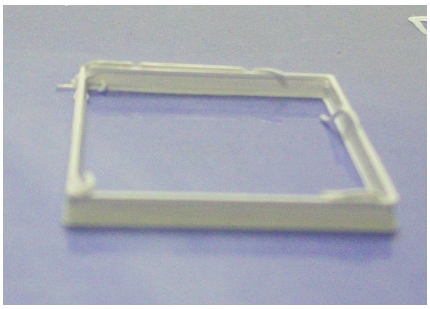

(a)

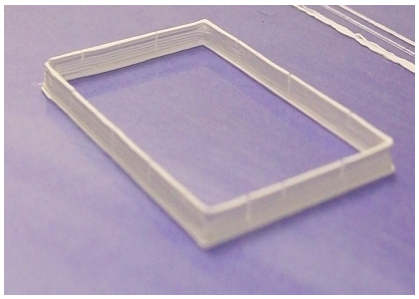

(b)

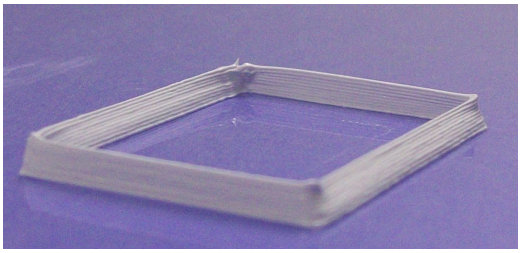

(c)

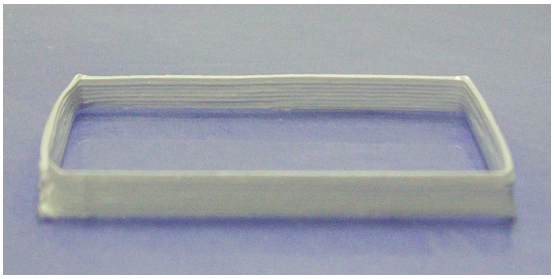

(d)

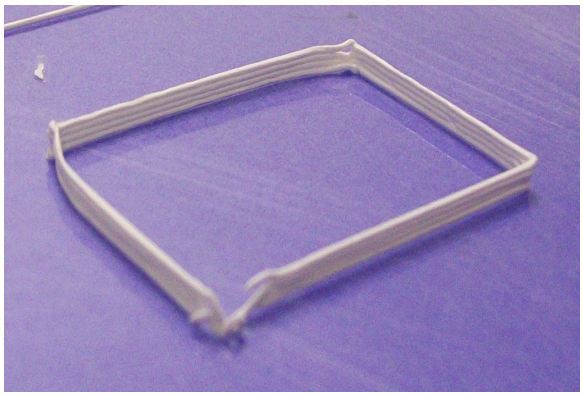

(e)

Figure 30: Fabricated Alumina thin walled rectangles for Standoff Distances of (a) 45%, (b) 50%, (c) 55%, (d) 60%, and (e) 65% of the Extrudate Diameter. Extrusion force is 450 N. Table velocity is 4.9 mm/s. Trajectory EOD method is used.

(a)

(b)

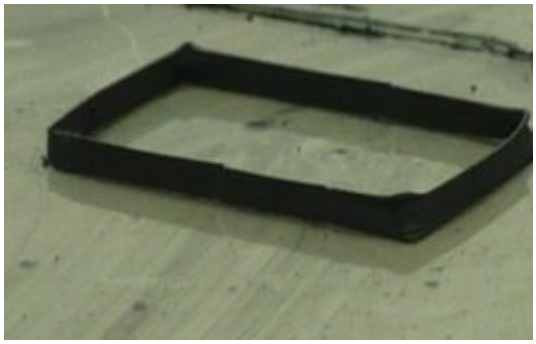

(c)

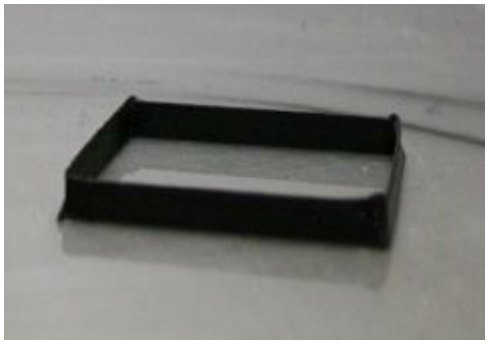

(d)

(e)

Figure 31: Fabricated Zirconium Diboride Thin Walled Rectangles for Standoff Distances of (a) 45%, (b) 50%, (c) 55%, (d) 60% and (c) 65% of the Extrudate Diameter. Extrusion Force is 150 N. Table Velocity is 5.3 mm/s.

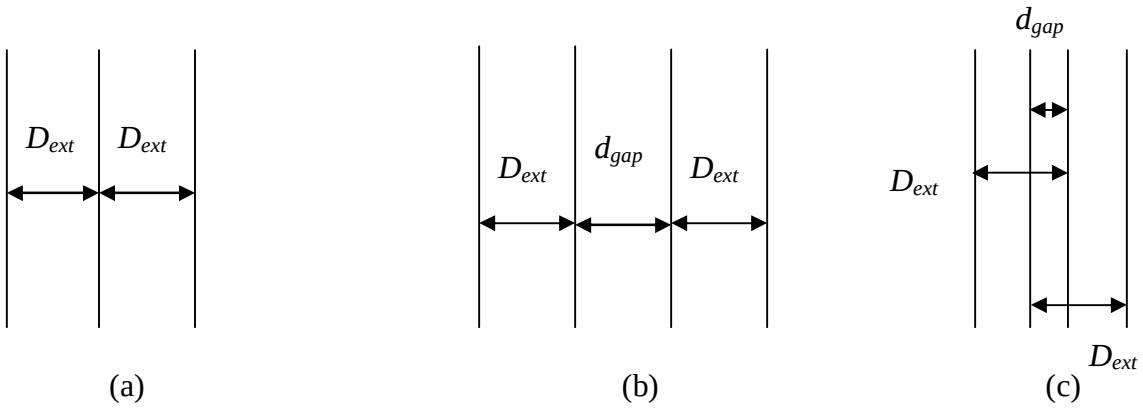

Figure 32: Diagrams Showing Overlap Factors that are (a) Zero, (b) Negative and (c) Positive.

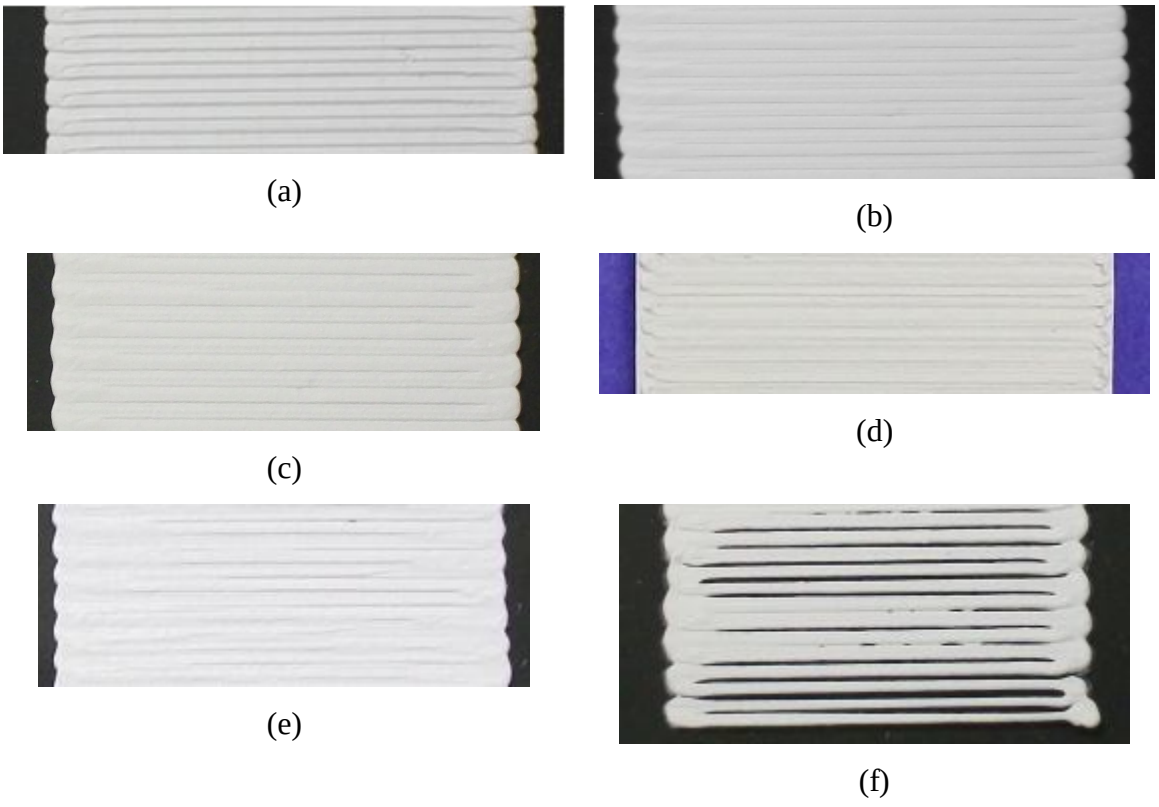

Figure 33: Rastering Conducted with Alumina and Overlap Factors of (a) -30%, (b) -35%, (c) -40%, (d) -45%, (e) -50%, (f) -55%, and (g) -60% .Standoff distance is 55%.Extusion force is 450 N. Table velocity is 4.868 mm/s. EOD Dwell Method is used.

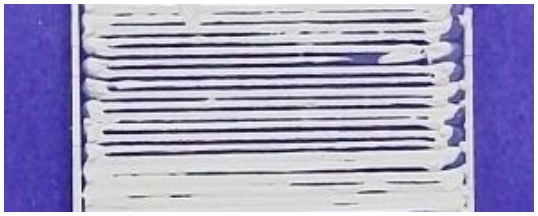

(g)

Figure 33 (continued): Rastering Conducted with Alumina and Overlap Factors of (a) -30%, (b) -35%, (c) -40%, (d) -45%, (e) -50%, (f) -55%, and (g) -60% .Standoff distance is 55%.Extusion force is 450 N. Table velocity is 4.868 mm/s. EOD Dwell Method is used.

(a)

(b)

(c)

(d)

Figure 34: Rastering Conducted with Zirconium Diboride and Overlap Factors of (a) -45%, (b) -50 %, (c) -55%, (d) -60% and (e) -65%. Standoff distance is 55%.Extrusion force is 150 N. Table Velocity is 5.3 mm/s. EOD Trajectory Method.

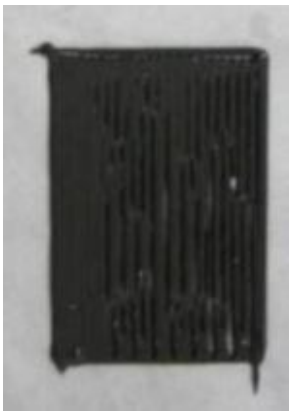

(e)

Figure 34(cont.): Rastering Conducted with Zirconium Diboride and Overlap Factors of (a) -45%, (b) -50 %, (c) -55%, (d) -60% and (e) -65%. Standoff distance is 55%.Extrusion force is 150 N. Table Velocity is 5.3 mm/s. EOD Trajectory Method is used.

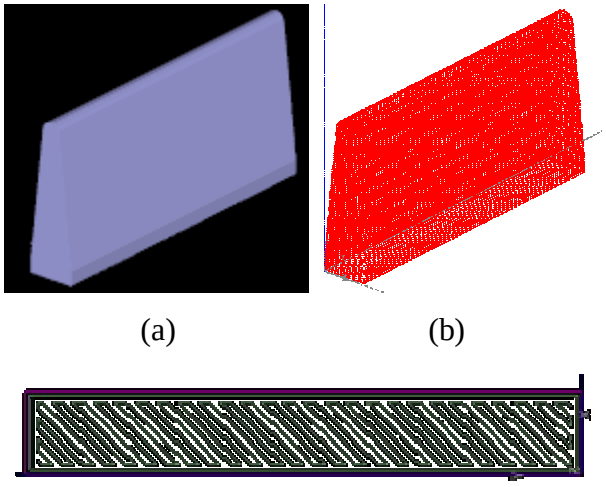

(a) (b)

(c)

Figure 35: Images from Insight 4.3.1 Part Slicing and Toolpath Generation software (a) .STL Model (b) Slices of .STL Model (c) Toolpath of one Slice of Simplified Fuel Injector Strut Part.

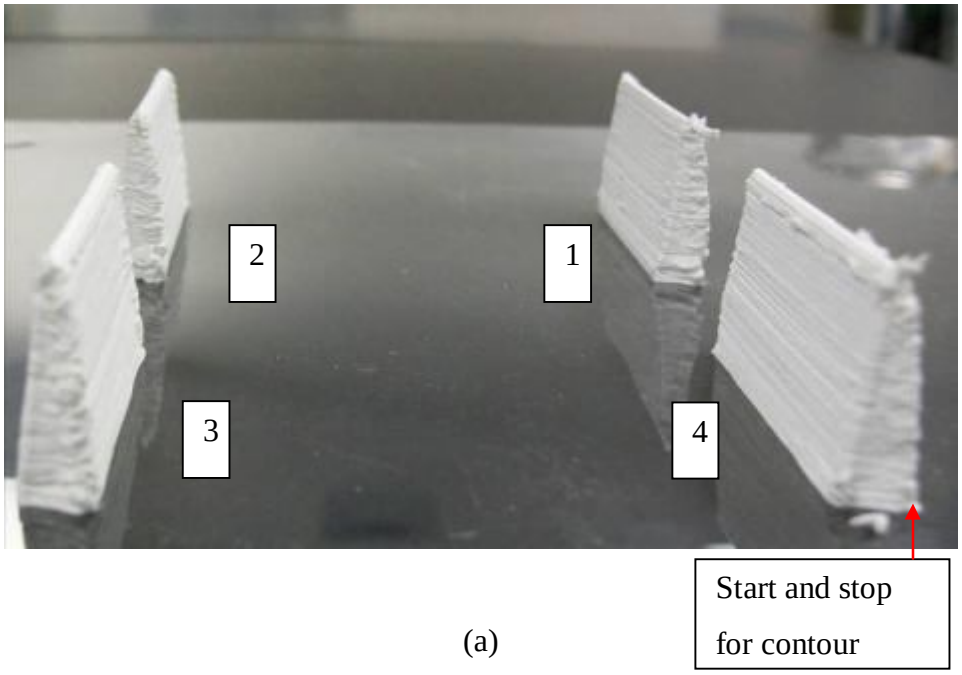

(a)

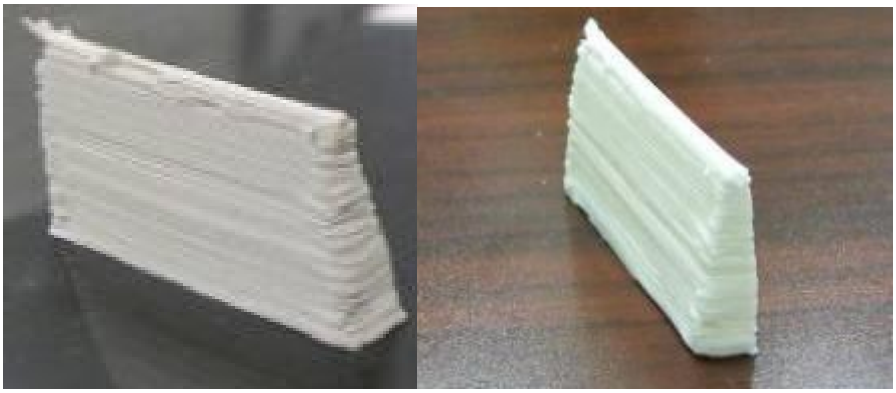

(b) (c)

Figure 36: (a)-(b) Fabricated Simplified Fuel Injector Strut using Alumina Paste. Dwell Time is 65%.Standoff Distance is 55%. Overlap Factor is 45%.Extrusion Force is 450 N.EOD Dwell Method. (c) Simplified fuel injector part (Alumina) after post processing.

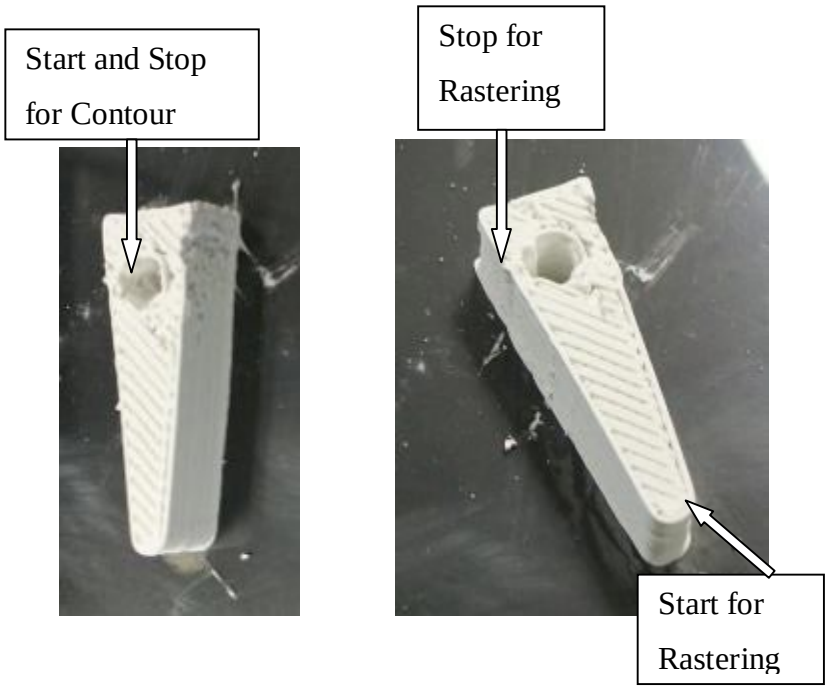

Figure 37: Parts Fabricated with Alumina Paste using the EOD Trajectory Method. Start Time is 4 s. Standoff Distance is 55%. Overlap Factor is 45%. Extrusion Force is 450 N.

(a) (b)

Figure 38: (a) Green Part (b) Sintered Part Fabricated using Zirconium Diboride Paste with EOD Dwell Method. Dwell 60%. Extrusion Force is 150 N. Overlap Factor is 55%. Standoff Distance is 55%.

(a) (b)

Figure 39: Cross Sections made with Zirconium Diboride Paste. EOD Trajectory Method. Start Time 2 s. Extrusion Force is 150 N. Overlap Factor is 55%. Standoff Distance is 55%.

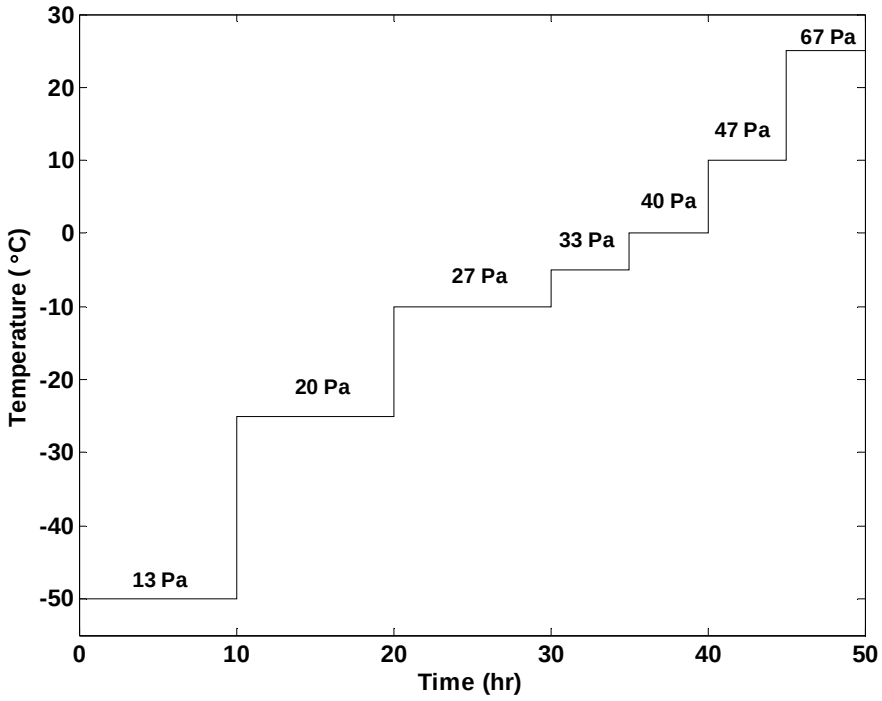

Figure 40: Freeze Drying Schedule for Zirconium Diboride

2. SUMMARY, CONCLUSIONS AND FUTURE WORK

The process of Extrusion on Demand (EOD) for ultra high temperature ceramics using Freeze-form-Fabrication has been discussed. Ceramic pastes consisting of alumina and zirconium diboride have been used. Process modeling is conducted. Experiments are done to design a controller. The extrudate velocity and diameter measurements are done. Data from these experiments is used to check the model fit using least. Experiments have been conducted to test for process parameters like standoff distance, overlap factor, start times and start dwells. Green parts have been fabricated using EOD and post processing has been conducted on these green parts.

From the experiments conducted it can be concluded that the extrusion process can be modeled as first order process. The integral control in the general tracking controller accounts for the variability in paste properties between batches, air pockets in the paste etc. The controller is capable of achieving a faster response with a ramp input as compared to a step input. The time constant for alumina paste is greater compared to zirconium diboride paste as it is more viscous. As alumina is more viscous the gain is lower than zirconium diboride i.e. more force is required to obtain same velocities. The least squares fit for the data relating extrusion force to extrusion velocity for both pastes has R close to 1 indicating a good model. The difference in extrusion forces between alumina and zirconium diboride pastes is due to the different viscosities and shear exponents. The lower shear exponent for zirconium diboride indicates that the paste is more shear thinning. The dwell method of EOD is not capable of completely eliminating the excess material deposition at the

start-stop. Standoff distances required for part fabrication have to be lower than the deposition track height. Overlap factors have to be negative to accommodate the paste spreading into adjacent gaps. Values of process parameters from these working ranges have been used to fabricate test bars, cross sections with holes, three dimensional simplified fuel injector parts.

Experiments will be conducted with different nozzle sizes. Fabrication of internal features in more than one orthogonal direction will require use of support material. Study of possible support materials will be done. The feasibility of implementation of multi-nozzle system may be necessary for support material will be studied.

VITA

Parimal Sanjay Kulkarni was born in Mumbai, India on December 5, 1984. She received her Bachelor of Engineering degree in Mechanical Engineering in June 2006 from the Pune University, Pune, India.

She worked as a Design Engineer from TESPL, Pune from August 2006 to May 2007. Her area of work covered thermal designing and CAD.

She started her study for her Master's degree in Manufacturing Engineering at Missouri University of Science and Technology (previously University of Missouri, Rolla) in August 2007. She received her Master's degree in December 2009. Her area of research has been in the field of additive manufacturing.